universität wien

MASTERARBEIT | MASTER'S THESIS

Titel | Title

A glimpse inside the viral factory
Revealing the spatial organization of transcription and translation in Mimivirus factories and the potential role of liquid-liquid phase separation

verfasst von | submitted by

Lotte Mayer BSc

angestrebter akademischer Grad | in partial fulfilment of the requirements for the degree of

Master of Science (MSc)

Wien | Vienna, 2025

Studienkennzahl lt. Studienblatt | Degree programme code as it appears on the student record sheet:	UA 066 865
Studienrichtung lt. Studienblatt | Degree programme as it appears on the student record sheet:	Masterstudium Molecular Biology
Betreut von | Supervisor:	Ass.-Prof. Dr. Anouk Willemsen

Acknowledgments

First and foremost, I want to thank Ass. Prof. Anouk Willemsen for being my supervisor for the last 4.5 years, for giving me so many opportunities and always believing in me. Secondly, I want to thank Junior Prof. Hugo Bisio for hosting me during my internship, helping me gain confidence with a lot of new skills in a new environment and making me feel welcome every step of the way. I am greatly looking forward to continuing being both of your students!

I also want to thank Prof. Matthias Horn and Prof. Jillian Peterson for taking the time to be on my thesis committee.

And last but not least I want to thank my friends and family. Thank you for listening to me talk about this work endlessly, for supporting me and being my haven during stressful times. Especially to my parents, who have been my biggest supporters from the start!

Abstract

Spatial separation of transcription and translation is one of the hallmark features of eukaryotes, facilitated by the nucleus. In recent years, however, viral structures were described that appear to have structural and functional similarities to the nucleus, and a spatial separation of transcription and translation has been proposed. Many giant viruses replicate in the cytoplasm in so-called viral factories. The architecture and spatial organization of many replication steps remain obscure to this day. The Mimivirus factory has been shown to be made up of two biomolecular condensates called the outer and inner layers. In this thesis, we investigate the progression of the outer layer throughout the infection to better understand the architecture of the viral factory and the potential role of this condensate. We have developed a single-molecule *in situ* hybridization protocol to specifically target Mimivirus messenger RNA (mRNA), allowing us to visualize mRNA localization in late-stage infections. Combined with bio-orthogonal amino acid tagging and ribosomal RNA fluorescence *in situ* hybridization we were able to distinguish between transcription and translation. We thereby show spatial separation of transcription and translation and provide preliminary evidence linking the outer layer condensate to these processes. This thesis provides novel tools for studying giant virus infections in the future as well as insights into the architecture and inner workings of the viral factory.

Zusammenfassung

Die räumliche Trennung von Transkription und Translation ist eines der charakteristischen Merkmale von Eukaryoten, das durch den Zellkern ermöglicht wird. In den letzten Jahren wurden jedoch virale Strukturen beschrieben, die funktionelle und strukturelle Ähnlichkeiten mit dem eukaryotischen Zellkern aufweisen, und für die eine räumliche Trennung von Transkription und Translation postuliert wurde. Viele Riesenviren replizieren im Zytoplasma der Wirtzelle in sogenannten viral factories. Die Architektur und räumliche Organisation vieler Replikationsschritte innerhalb dieser viral factories ist bis heute unklar. Es wurde gezeigt, dass die Mimivirus viral factory aus zwei biomolekularen Kondensaten besteht, die als äußere und innere Schicht bezeichnet werden. In dieser Arbeit untersuchen wir die Entwicklung der äußeren Schicht im Laufe der Infektion, um die Architektur der viral factory und potenzielle Rollen dieses Kondensats besser zu verstehen. Wir haben ein Protokoll zur single molecule *in situ* hybridization (smFISH) entwickelt, das spezifisch virale messenger RNA (mRNA)markiert und es uns ermöglicht mRNA-Lokalisierung in späten Infektionsstadien sichtbar zu machen. In Kombination mit bio-orthoginal amino acid tagging und FISH an ribosomaler RNA der Wirtzelle sind wir in der Lage Transkription und Translation visuell zu unterscheiden. Mit diesen Methoden zeigen wir eine räumliche Trennung von Transkription und Translation. Wir liefern außerdem erste Hinweise, dass die äußere Schicht in diesen Prozessen involviert ist. Diese Arbeit liefert neue Werkzeuge für die Erforschung von Riesenvirusinfektionen sowie Einblicke in die Architektur und Abläufe im inneren der viral factory.

List of abbreviations

MOI	multiplicity of infection
h.p.i.	hours post infection
OLS1	outer layer scaffold 1
ILS1	inner layer scaffold 1
FRAP	fluorescence recovery after photobleaching
CLSM	confocal laser scanning microscope
(sm)FISH	(single molecule) fluorescence *in situ* hybridization
mRNA	messenger RNA
DAPI	4',6-Diamidino-2-phenylindole
EdU	5-Ethinyl-2'-Desoxyuridin
HPG	Homopropargylglycin
BONCAT	bio-orthogonal non canonical amino acid tagging
FUNCAT	fluorescent non-canonical amino acid tagging
DiD	1,1'-dioctadecyl-3,3,3',3'- tetramethylindodicarbocyanine, 4-chlorobenzenesulfonate salt
VF	viral factory
eVF	early viral factory
mcp	major capsid protein
IDP	intrinsically disordered protein
IDR	intrinsically disordered region
dPCR	digital Polymerase chain reaction

1 Introduction 6
1.1 Introducing giant viruses 7
1.1.1 Mimivirus infection and replication 8
1.1.2 Similarities of the viral factory and the eukaryotic nucleus 8
1.2 Liquid-liquid phase separation 9
1.2.1 The role of intrinsically disordered proteins 9
1.2.2 Liquid-liquid phase separation in cellular processes 10
1.3 Aim of the thesis 11
2 Results 12
2.1 mRNA localization changes during the infection cycle 12
2.2 Translation occurs at the periphery of the viral factory 14
2.3 Outer layer changes spatial distribution and biophysical properties throughout the infection 17
2.3.1 Changes in spatial distribution 17
2.3.2 Changes in biophysical properties 18
2.4 Outer layer sub-compartments have different biophysical properties 20
2.5 mRNA colocalizes with the outer layer scaffold 1 21
2.6 MOI influences number of transcription sites in late-stage viral factories 23
3 Discussion 25
4 Methods 28
4.1 Fluorescence recovery after photo-bleaching (FRAP) 28
4.1.1 Sample preparation 28
4.1.2 Imaging 28
4.1.3 Analysis 28
4.1.4 Remaining problems in data analysis and interpretation 29
4.2 Fluorescent stainings 31
4.2.1 Sample preparation 31
4.2.2 Fluorescent noncanonical amino acid tagging 31
4.2.3 Single-molecule messenger RNA fluorescence *in situ* hybridization 32
4.2.4 Ribosomal RNA fluorescence *in situ* hybridization 35
4.2.5 DiD staining 35
4.2.6 Imaging 35
4.3 MOI experiments 36
4.3.1 Digital polymerase chain reaction (dPCR) 36
4.4 Statistics and data visualizations 36
5 Supplementary information 37

1 Introduction

The jump from prokaryotes, bacteria and archaea, to eukaryotes is largely a matter of size and its subsequent implications. Eukaryotic cells are 3-4 orders of magnitude larger than prokaryotic cells[1]. This means that proteins and molecules within the cell need to be trafficked more efficiently, and the cell often needs to be compartmentalized[2 3].

While prokaryotes do show compartmentalization it is not to the same extent as is the case for eukaryotes. Although some bacteria possess lipid bound compartments necessary for carbon fixation or photosynthesis and even around the chromosome[4 5 6] these structures do not occur universally in prokaryotes. Meanwhile, eukaryotes all share a certain internal structure composed of an endomembrane system, mitochondria and a nucleus. The characteristic membrane bound organelles are one well described way for the cell to spatially organize metabolic functions[7]. Another way for cells to achieve compartmentalization is through so-called liquid-liquid phase separation. This is a relatively novel concept that has gained traction in recent years. It relies on protein interactions creating membrane-less organelles also referred to as biomolecular condensates that concentrate certain molecules to facilitate reactions[8].

The spatial separation of transcription and translation is a hallmark of eukaryotes brought forth by the nucleus. Prokaryotes are known for their coupled transcription and translation forming RNA-Polymerase – mRNA – ribosome complexes[9]. This means that ribosomes bind nascent mRNA before transcription is terminated to begin translation[10]. In eukaryotes transcription occurs in distinct locations inside the nucleus called “transcription factory”[11] and translation occurs outside of the nucleus at the rough endoplasmic reticulum (RER) or in the cytoplasm[12]. That allows mRNAs to be processed inside the nucleus prior to translation ensuring only mature mRNAs are translated[13].

While this spatial separation was long considered a phenomenon solely associated with eukaryotes recent discoveries have shown functionally similar structures in viruses[14 15 16].

1.1 Introducing giant viruses

Viruses were long defined via their small particle sizes, condensed genomes and parasitic nature. Their genomes were believed to be reduced to the minimum and to not encode any elements for protein synthesis machinery or metabolic pathways[1718]. Historically scientists filtered samples to exclude everything larger than known viruses when looking for novel viruses introducing a sampling bias and excluding anything defying this definition.

The first isolation of a so-called giant virus comes from a cooling-tower sample of a pneumonia outbreak in 1992[19]. At that time, it was believed to be a bacterium due to its size and reaction to gram staining. In 2003 however this was identified as an unusually large virus with a capsid size of 400-500 nm[20], a genome of 1.2 megabases and many orphan genes. But most astonishingly it was later found that this virus encodes for genes related to translation like elongation and initiation factors and even tRNAs[21]. In the years following the discovery of Mimivirus the hunt for other giant viruses uncovered a huge diversity of novel viruses with previously unthinkable properties persistently challenging current views on viruses[22].

The subsequently discovered viruses are now grouped under *Nucleocytoviricota* which is a phylum of large DNA viruses most of which can replicate in the cytoplasm[23]. This is a very diverse phylum including *Poxviridae*, *Asfarviridae*, *Iridoviridae*, *Phycodnaviridae*, *Marseilleviridae* and *Mimiviridae*[24] which are found in a wide range of environments[25].

Unsurprisingly these different viruses also employ different replication tactics. While many of them have cytoplasmic replication stage creating a nuclear like environment called the viral factory, some viruses like Noumeavirus recruit nuclear replication factors during early-stage infection[26] or even initiate replication in the nucleus (*Asfarviridae*[27]) before moving to the cytoplasm, while others like Mimivirus and Tupanvirus do not rely on the nucleus whatsoever[28] [29]. A minority of giant viruses has also been described to replicate in the nucleus which can cause large restructuring of the nucleus[30] [31].

1.1.1 Mimivirus infection and replication

Mimivirus, as well as many other giant viruses[32], replicates in the cytoplasm. It enters the cell via phagocytosis and upon infection the viral particle releases a core through the so-called stargate structure[33]. Early transcription is shown to be initiated in this core. DNA replication around the site in which each core releases its contents establishes an early viral factory. Each viral particle establishes one early viral factory which later fuse to become a single mature factory[34]. The architecture of these factories has remained enigmatic for a long time. Studies showed assembly of rough endoplasmic reticulum (RER) cisternae in proximity to the factory at 7-8 hours post infection[35] but further characterization of the architecture and internal workings of the viral factory is still lacking. In a recent study, Rigou et al.. have shown evidence that these factories are composed of at least two distinct biomolecular condensates[36]. This can partly explain how early viral factories appear to first cluster and then fuse in early stages of infection. The two condensates were termed inner and outer layer which are shown to be made up by the Inner Layer Scaffold protein (ILS1) and Outer Layer Scaffold protein (OLS1), respectively. The same study also provides evidence that DNA associates to the ILS1 which co-localizes with the viral factories while the OLS1 forms a layer around unfused factories facilitating the fusion process[37]. Associated with the OLS1 they found ribosomal proteins and eukaryotic translation initiation factors suggesting this condensate might play a role in mRNA processing and translation regulation[38]. A previous study has shown mRNA accumulation in sites adjacent to early viral factories containing replicating DNA during early stages of replication[39], however the spatial distribution of transcription and translation especially during later stages remains to be elucidated.

1.1.2 Similarities of the viral factory and the eukaryotic nucleus

The Mimivirus viral factory is a DNA-dense cytoplasmic structure that reaches roughly the size of a nucleus[40]. It is independent of the host nucleus and created by the virus for its own replication. Throughout the cycle the initial early viral factories coalesce into one mature one that can grow until cell lysis. After around 8 h.p.i. it reaches a size similar to the host nucleus. Around this time during the infection membranes studded with ribosomes are recruited to the periphery of the factory[41]. This creates an environment showing substantial structural similarities to the nucleus. DNA is replicated within the factory while it is surrounded by a membrane with ribosomes associated. Liquid-liquid phase separation appears to play an important role in the development and maintenance of the viral factory[42]. While the nucleus is membrane bound liquid-liquid phase separation is also known to play an important role in nuclear sub-compartmentalization[43].

In addition to the described structural similarities there have been reports on functional similarities of the viral factory and the nucleus. Marseillevirus has been found to encode histone doublets[44]. These are localized in the viral factory as well as inside the packaged viral particles. This shows a non-eukaryotic organism with this DNA packaging mechanism[45].

Mimivirus has been shown to harbour genes related to translation and possesses mRNA capping machinery[46] [47]. This is widely considered a hallmark of the eukaryotic transcription translation system as it plays a role in the uncoupling of these processes. The presence of these enzymes and subsequently possible ability to process their own mRNAs[48] suggests a transcription-translation system more similar to eukaryotes.

Whether transcription and translation are truly separated during Mimivirus infection and where they take place remains to be investigated.

1.2 Liquid-liquid phase separation

Cells have to orchestrate many reactions in parallel efficiently. To that end they have developed specific membrane enclosed compartments that allow spatial partitioning of important reactions. Still there are many reactions happening in the cytoplasm and within these spaces that need to be tightly regulated. These reactions are frequently regulated by compartments that are made up by liquid-liquid phase separation[49]. These membrane-less organelles also referred to as biomolecular condensates have liquid-like properties. They can rapidly fuse, divide and dissolve in response to environmental factors[50] [51]. Condensates can also vary in fluidity from liquid to gel-like and can become almost solid. The degree of fluidity is directly correlated with the condensates function[52].

The first description of biomolecular condensates came from *Caernohabditis elegans*. In 2009 Li P. et al. described P granules as liquid-like drops that can fuse and behave similarly to water.[53] Since then more cases of this phenomenon have been described, and it has been connected to various diseases from cancer[54] to neurological disorders like amyotrophic lateral sclerosis[55].

1.2.1 The role of intrinsically disordered proteins

Many condensates are made up of intrinsically disordered proteins[56] without them interacting with binding partners. The ability of an intrinsically disordered protein (IDP) to undergo phase separation is highly dependent on its composition. Interactions contributing to phase separation induced by IDPs range from pi-pi interactions to electrostatic interactions[57] or can be mediated by potential low complexity segments in the disordered region[58] [59].

Intrinsically disordered regions often contain many modification sites. Depending on the modification they can affect structure, hydrophobicity and charge of the region which in turn affects how the protein interacts with the environment, creating or destroying interaction sites. The cell can use this to mediate the properties of biomolecular condensates in response to environmental changes[60]. Different post translational modifications have different effects on the condensates. These effects only vary depending on the modification but also on the residue. Phosphorylation can modify the behaviour and sub-compartmentalization of condensates[61] while methylation often plays a role in either the dissolution or the

assembly of condensates[27 62]. The dynamic of these modifications is used by the cell to modify the properties of the condensate allowing even for a switch in function[63 64].

1.2.2 Liquid-liquid phase separation in cellular processes

One of the fundamental processes regulated by liquid-liquid phase separation in eukaryotic cells is transcription. Transcription in eukaryotes occurs in the very packed complex environment of the nucleus and must therefore be highly regulated. While the functional mechanisms have been studied in a lot of detail the spatial organization has remained an open question for a long time.

It has already been shown in 1993 that transcription takes place at discreet sites inside the nucleus instead of an even diffusive distribution[65]. These sites have been referred to as transcription factories[66] and are known to have higher concentrations of RNA Polymerase 2[67]. In recent years this distinct spatial organization has been linked to liquid-liquid phase separation showing that phase separation plays a role in defining these sites and controlling gene expression[68 69]. Similarly, evidence shows RNA Polymerase clustering associated with liquid-liquid phase separation in certain stages of the life cycle in E. coli[70]. Liquid-liquid phase separation has further been shown to play a crucial role in chromatin organization[71]. It is a relevant player in chromatin condensation, loop extrusion and nuclear compartmentalization[72].

But not only the cell can utilize liquid-liquid phase separation. Pathogens, especially viruses, are known to create environments favourable for their own replication within host cells to help them replicate efficiently. This has been shown to be the case for Influenza A[73] as well as SARS-Cov 2[74] and Measles virus[75]. For different viruses this can look different. A striking example is the Mimivirus factory. As previously mentioned Mimivirus creates a biphasic viral factory upon infection. The two phases, the inner and outer layer, are made up by scaffold proteins called inner layer scaffold 1 (ILS1) and outer layer scaffold 1 (OLS1). It has been shown that ILS1 forms condensates in the presence of linear and circular DNA[76] and has been observed to associate with the DNA in viral factories[77]. OLS1 has been shown to play a role in the coalescence of early viral factories and has been suggested to be involved in translation and mRNA processing. The phenomenon of liquid-liquid phase separation forming cytoplasmic viral factories has further been shown to be the case in many other *Nucleocytoviricota*[78].

1.3 Aim of the thesis

The architecture and inner workings of the Mimivirus viral factory have remained elusive after more than 20 years of research on giant viruses. While there are several papers suggesting a spatial separation of transcription and translation, no direct evidence has been given to date. In this thesis we aim to elucidate the spatial organization of transcription and translation during late-stage infection. Furthermore, by characterizing the outer layer condensate, we aim to gain insights into the structural and potential functional changes the viral factory undergoes throughout the course of a Mimivirus infection.

Due to the recent discovery, not many protocols specifically tailored towards studying giant viruses are available. In this thesis we therefore aim to establish a single molecule mRNA fluorescence *in situ* hybridization (smFISH) protocol targeting viral mRNA in amoeba host cells. As the spatial distribution of transcription and translation during giant virus infections especially at late stages of infection has not been shown yet we aim to visually distinguish the two processes using our smFISH combined with other methods to label proteins and nucleic acids (BONCAT, and DAPI). This protocol allows us to gain novel information on the inner workings of the viral factory. In addition, we will track the restructuring of cellular membranes throughout the infection. This will provide insights into the availability of ribosomes during different timepoints as well as visualizing membrane structures associated with the viral factory.

We further aim to characterize the outer layer of the viral factory throughout the full infectious cycle. This will show how the condensate changes on a cell biological basis as well as biophysically. We will gain insights into changes of the factory's architecture as well as potential functions of the outer layer.

Overall, this thesis will provide novel insights into the regulation of important processes like transcription and translation in the viral factory and how this unique structure progresses and changes throughout the infectious cycle.

2 Results

2.1 mRNA localization changes during the infection cycle

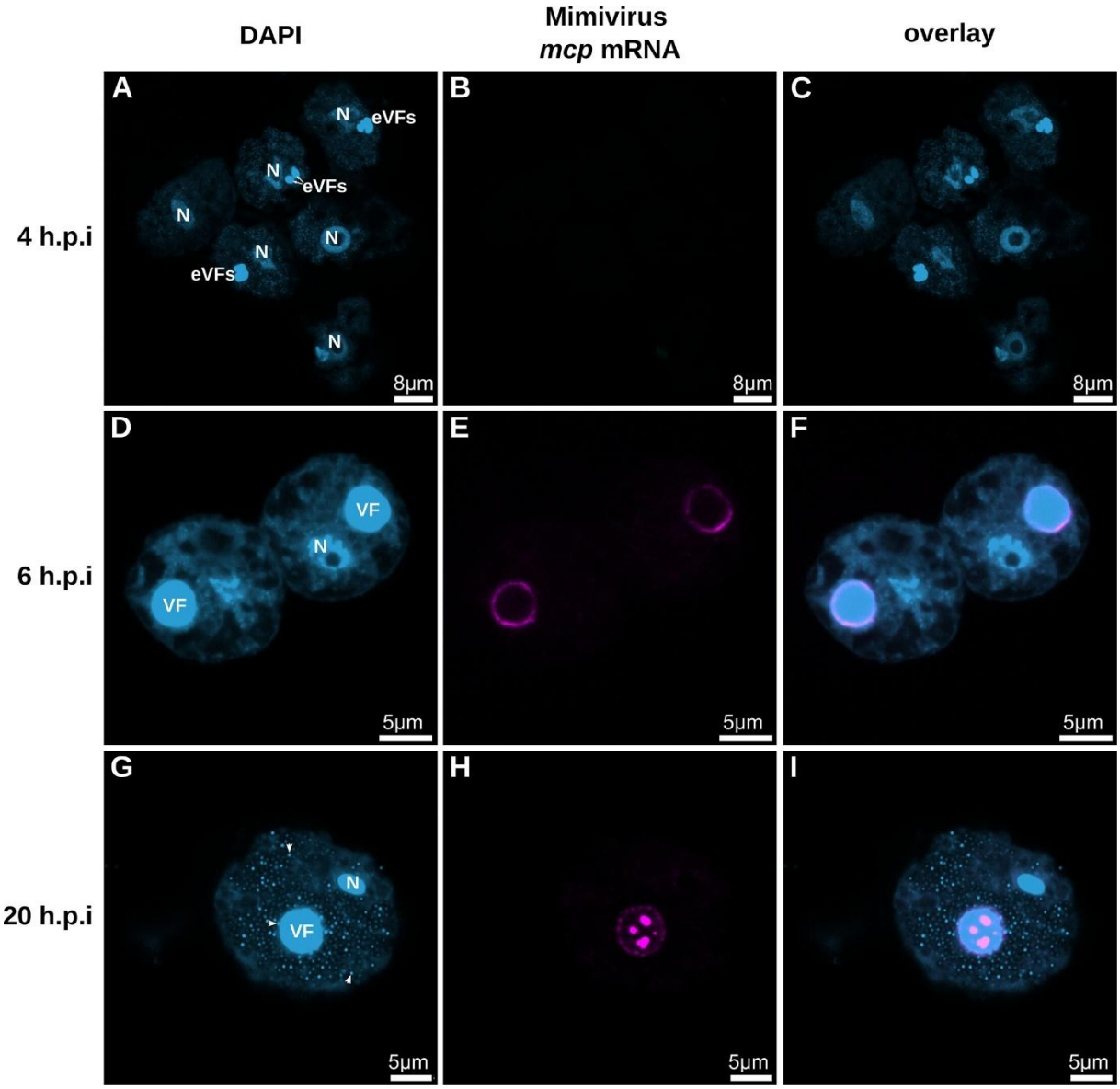

Figure 1: Mimivirus mcp mRNA localizes at different sites during the course of infection. *(**A, B, C**) Cells were infected with an MOI of 0.5 and harvested at 4 h.p.i. (**A**) DAPI staining (light blue) of six amoeba cells, of which three are infected. A brighter DAPI signal can be observed in the nucleus (N) and the early viral factories (eVFs) of the cells. (**B**) No Mimivirus mcp mRNA signal (magenta) is visible at 4 h.p.i. (**C, F, I**) Overlay of DAPI staining (light blue) and Mimivirus mcp mRNA signal (magenta). (**D, E, F**) Cells were infected with an MOI of 0.5 and harvested at 6 h.p.i. (**D**) DAPI staining (light blue) of two infected amoeba cells. (**E**) Mimivirus mcp mRNA signal (magenta) is localized around the viral factories. (**G, H, I**) Cells were infected with an MOI of 1 and harvested at 20 h.p.i. (**G**) DAPI staining (light blue) of one infected amoeba cell. A brighter DAPI signal can be observed in the nucleus (N), the viral factory (VF), and the viral particles (white arrows indicate three examples) within the cell. The viral particles can be observed budding out of the viral factory and within the rest of the host cell. (**H**) Mimivirus mcp mRNA signal (magenta) of one infected amoeba cell at 20 h.p.i. is localized surrounding and at specific spots within the viral factory. The scale bars are drawn on top of the original ones for visibility. This image is part of already published work from the defendant [https://doi.org/10.1128/jvi.00554-25]*

Previous studies have combined electron tomography and fluorescence microscopy to show that each viral core establishes an early viral factory after being released into the cytoplasm and that those early viral factories can fuse to become a mature viral factory

at later stages of infection[79]. Incubating the infected cells with bromodeoxyuridine (BrdU) which is incorporated into DNA during replication Mutsafi et al. were able to show that DNA replication occurs in the host cytoplasm after the exit of the Mimivirus genomes from the viral cores[80]. In the same study they propose that early transcription is initiated in the viral cores and used bromouridine (BrU) which is incorporated in newly synthesized mRNA to show mRNA accumulation at discrete sites in the cytoplasm adjacent to the sites of DNA replication[81]. Their findings suggest that transcription during early timepoints may take place outside of the viral factory. The mRNA is however still found in the periphery of the early viral factories leading us to believe it may be within the outer layer condensate. To better understand the intracellular localization of Mimivirus *mcp* mRNA during infection, we use the newly developed smFISH method.

Acanthamoeba terricola Neff host cells were infected with Mimivirus, and the cells were harvested at different time points during the infection cycle. Consistent with the results described previously we observe multiple early viral factories at the intermediate timepoint 4 h.p.i. and a big mature one during later stages of infection (>6 h.p.i.) (Fig.2). We observe signal from our *mcp* mRNA probes only starting at 6 h.p.i. (Fig. 1E), not yet at 4 h.p.i. (Fig. 1B), which is in line with the transcriptomic data[82]. We observe signal from our probes up until shortly before cell lysis (12-20 h.p.i.). Interestingly, the signal distribution at 6 h.p.i. is different from the later stages. Shortly after fusion of the viral factories (6 h.p.i.) the mRNA can only be observed as a ring around the viral factory (Fig. 1E). In later stages of infection however we consistently observe mRNA accumulation in discrete sites within the viral factory as well as mRNA localised in the ring around it (Fig. 1H). This distribution indicates that transcription takes place within these discrete sites while translation may occur at the periphery of the mature viral factory[83].

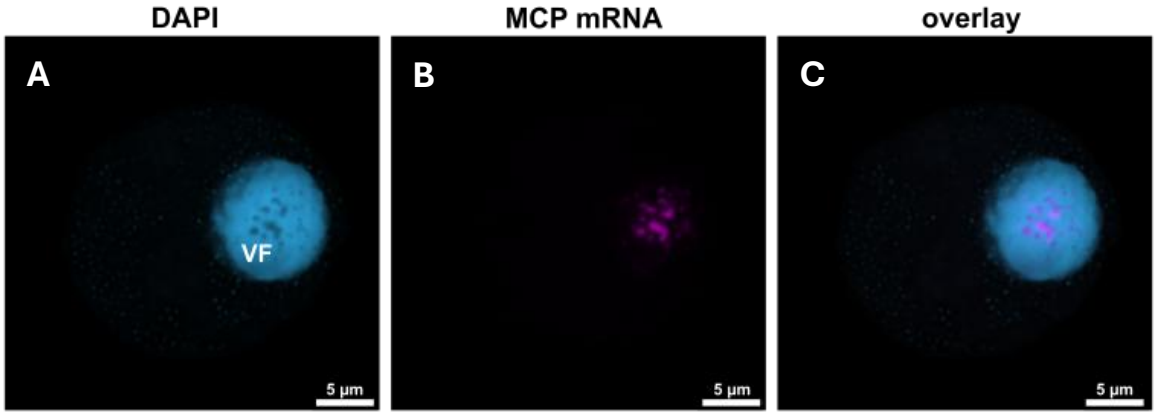

Figure 2: mRNA localizes in distinct sites of lower DAPI signal inside the mature viral factory. ***(A)*** *The late-stage viral factory showing multiple distinct spots of lower signal intensity using DAPI staining (light blue). In* ***(B)*** *viral mRNA is depicted in magenta.* ***(C)*** *The overlay shows the sites exhibiting lower DAPI signal appear to be filled with viral mRNA. This image is part of the supplementary material of already published work from the defendant [https://doi.org/10.1128/jvi.00554-25].*

Morphological changes of the viral factory are not reduced to the fusion of early viral factories to mature factories. It is also noteworthy that after fusion the DAPI staining of the factory is very strong and even while later stages of infection (>12 h.p.i.) show uneven

staining with distinct holes observed in the factory. These sites are where we consistently observed the mRNA to localise.

2.2 Translation occurs at the periphery of the viral factory

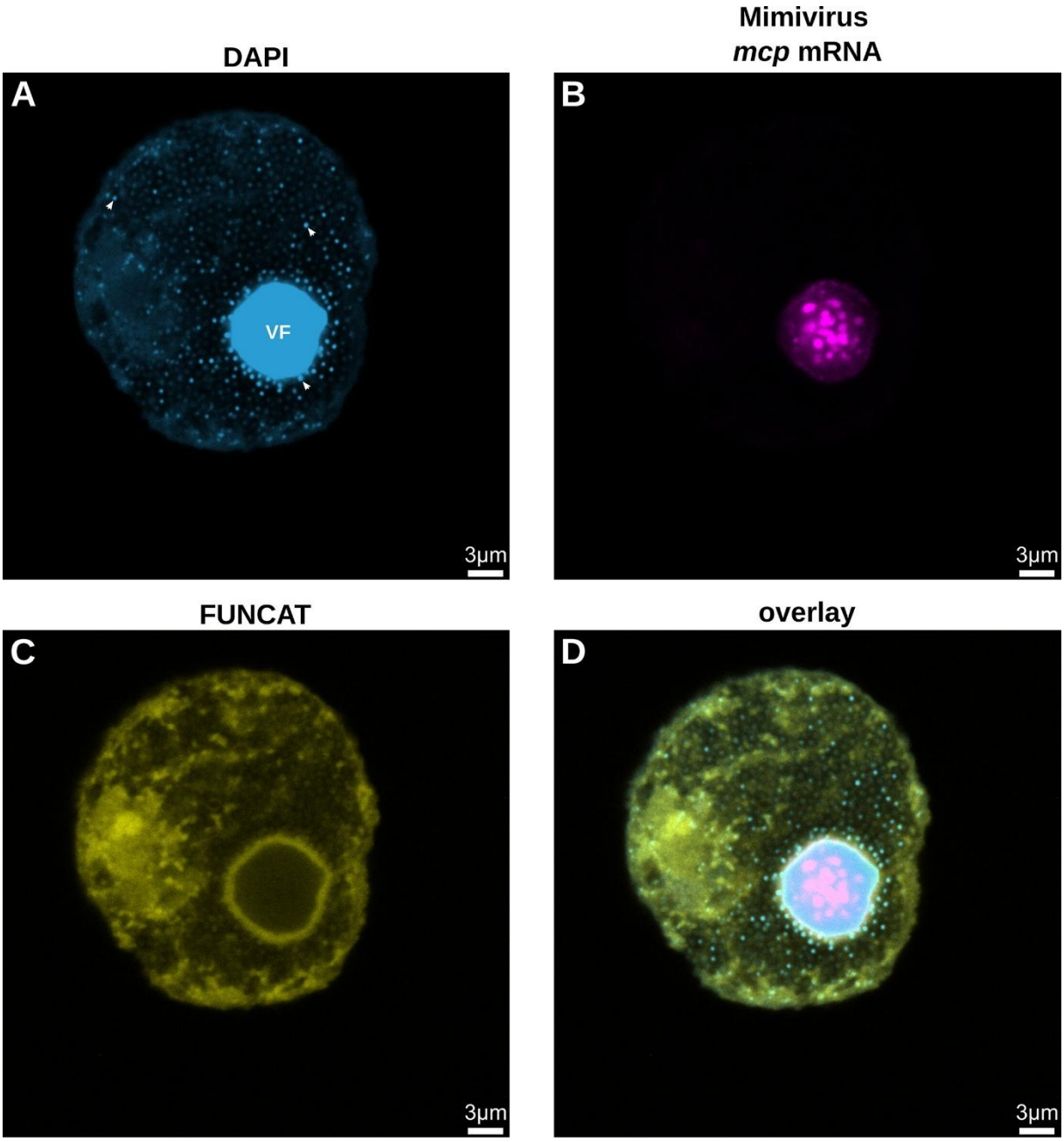

Figure 3: Translation localization coincides with mRNA localization surrounding the viral factory at late infection *stages. Cells were infected with an MOI of 1 and harvested at 21 h.p.i. (**A**) DAPI staining (light blue) of one infected amoeba cell. A brighter DAPI signal can be observed in the viral factory (VF) of the cell and for viral particles (white arrows indicate three examples) that can be seen budding out of the viral factory and filling the rest of the cell. (**B**) Mimivirus mcp mRNA signal (magenta) of the same cell as in panel A. The mRNA is localized surrounding the viral factories and at specific spots within the viral factories. (**C**) FUNCAT signal (yellow) of the same cell as in panel A. The strong FUNCAT signal suggests that the exported Mimivirus mRNA is translated here. (**D**) Overlay of DAPI staining (light blue), Mimivirus mcp mRNA signal (magenta), and FUNCAT (yellow) of the same cell as in panel A. For visibility, the scale bars are drawn on top of the original ones. This image is part of already published work from the defendant [https://doi.org/10.1128/jvi.00554-25]*

Following up on our previous results showing that exported mRNA remains near the viral factory (Fig. 1E), which suggests that viral translation might occur in this location, we have

combined the smFISH with bio-orthogonal non-canonical amino acid tagging (BONCAT). This method relies on the incorporation and subsequent visualization of Homopropargylglycin (HPG) in newly synthesized proteins[84] [85] [86] and is also frequently referred to as FUNCAT (fluorescent non-canonical amino acid tagging) [87] [88].

Our results show a ring around the factory where amino acids have been incorporated within the last 30 minutes. This ring co-localizes with the ring seen in our mRNA signal suggesting active translation of viral mRNA at this location (Fig. 3)[89]. Recent studies have shown that giant viruses and their known hosts frequently present a mismatch in codon usage[90]. It has been shown that mRNA stability heavily relies on codon optimality[91]. This opens the questions on how giant viruses can still replicate effectively despite the significant codon mismatch. Mimivirus, as well as many other giant viruses, encodes its own tRNAs. Recent data shows however, that the tRNA pool throughout the Mimivirus infection in *Acanthamoeba terricola* is not significantly altered[92]. It was therefore suggested that instead they create an environment favourable for viral translation in which the necessary tRNAs as well as ribosomes and translation factors will be enriched[93].

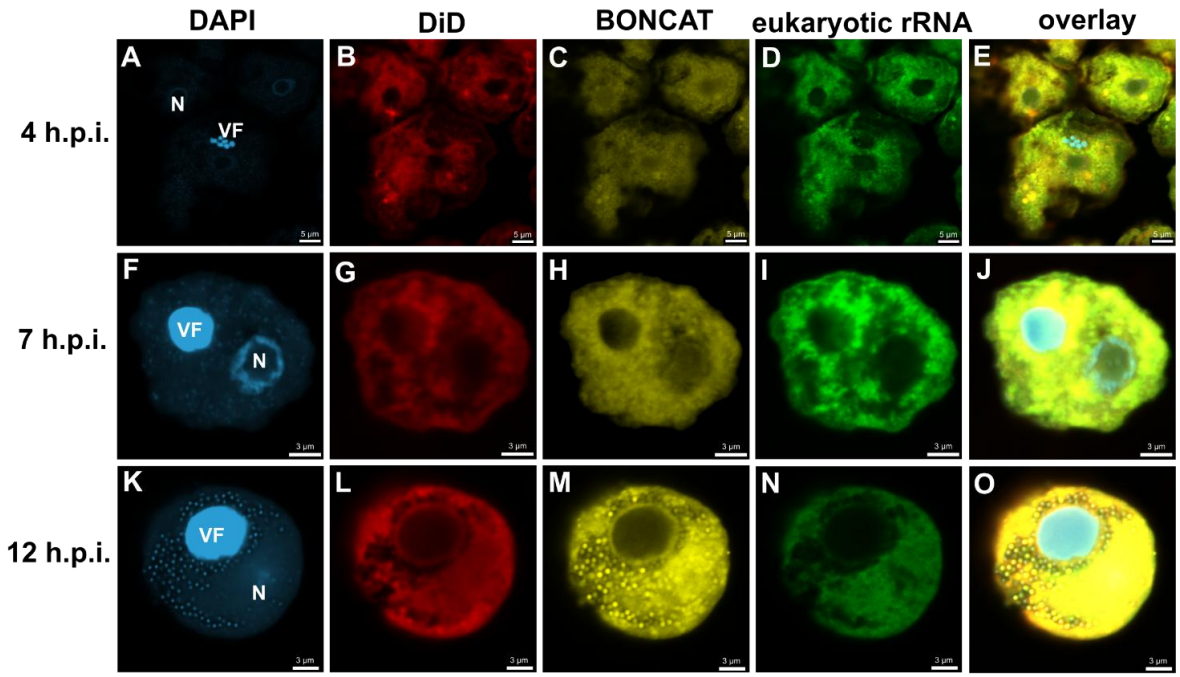

Figure 4: Restructuring of membranes and membrane recruitment to the factory in late-stage infection (A-E) *show the cells after 4 hours of infection with Mimivirus. Using the DiD staining (**B**) we can see that the area where the early factories cluster is a membrane-free hydrophilic environment. In (**C**) BONCAT signal shows accumulation of amino acids that have been incorporated within the last 30 minutes around the factories while rRNA FISH signal in (**D**) shows only very weak signal in the area of the factories. (**F-J**) show cells after 7 hours of infection. Notably here the DiD signal in (**G**) and the rRNA signal in (**I**) look almost identical. BONCAT in (**H**) shows an increase of signal intensity around the factory while the signal in the rest of the cell becomes weaker. However, a ring of BONCAT signal around the nucleus remains. (**K-L**) show. This image is part of the supplementary material of already published work from the defendant [https://doi.org/10.1128/jvi.00554-25]*

To further test this hypothesis, we performed FISH on ribosomal RNA tracking its localization throughout the infection. We combined this with FUNCAT and a lipophilic

carbocyanine DiD dye, which enhances fluorescence when incorporated into membranes or bound to lipophilic biomolecules such as proteins. The results show that in all the timepoints the rRNA and DiD signals are almost identical (Fig. 4 B&D, G&I, L&N) suggesting that most ribosomes remain membrane associated throughout the infection. At 4 h.p.i., we observe no membranes in the area where the early viral factories cluster (Fig. 4B) which is consistent with the evidence for liquid-liquid phase separation. After fusion of the factories, we can see membranes with ribosomes associated start assembling close to the viral factory (Fig. 4G) leading to a membranous ring around the factory overlapping with rRNA and FUNCAT signal at very late stages of infection (Fig. 4L-N). This signal likely indicates the host membranes known to be recruited to the VF[94]. These host membranes have the characteristic appearance of rough endoplasmic reticulum (ER). They are studded with ribosomes[47], further supporting the hypothesis that the translation of Mimivirus mRNA occurs at this ring surrounding the VF.

Comparing the appearance of the nucleus with that of the viral factory using these staining we can see certain similarities in these images. Both at 4 h.p.i. and 7 h.p.i. the nucleus appears as a dark area in DiD staining, BONCAT and rRNA FISH. At 7 h.p.i. when membranes are recruited to the factory, we observe less signal in the vicinity of the nucleus compared to 4 h.p.i. but instead we observe a faint ring around the nucleus with all stainings similar to our results from the mature viral factory at 12 h.p.i.. This indicates architectural and functional similarities of the viral factory and the eukaryotic nucleus.

2.3 Outer layer changes spatial distribution and biophysical properties throughout the infection

To understand the progression of the architectural changes in the viral factory and how they could be mediated by liquid-liquid phase separation we used live imaging to follow a full infectious cycle of Mimivirus in *Acanthamoeba terricola* Neff cells engineered to overexpress GFP-tagged OLS1[95], provided by our collaborator Hugo Bisio. The overexpressed viral protein indicates the localization of the outer layer condensate allowing us to get a full picture of the developmental changes of the factory throughout the infection.

2.3.1 Changes in spatial distribution

Our results in early and intermediate timepoints are consistent with the results previously describes in Rigou et al.. for 4 h.p.i. and 6 h.p.i.[96]. At 4 h.p.i. we observe clustered early viral factories that are surrounded by the OLS1 (Fig. 5A). This appears to create a shared environment for the viral factories while separating them from the cytoplasm of the host cell. After fusion of the factories the GFP-tagged OLS1 remains as a ring around the factory with only very little signal detected inside the factory (Fig. 5A). As the infection progresses OLS1 migrates into the viral factory around 10 h.p.i. completely filling the factory (Fig. 5A). The potential sub-compartment of the outer layer proceeds to condensate into distinct sites within the factory.

Interestingly the progression of spatial distribution of OLS1 throughout the infection shows strong similarities with the signal obtained using our mRNA-FISH protocol (Fig.1H). This suggests that mRNA may associate with the outer layer condensate. Combined with previous evidence showing that eukaryotic translation initiation factors associate with OLS1[97] this indicates that one of the potential roles of the outer layer may lay in the spatial organization of transcription and translation.

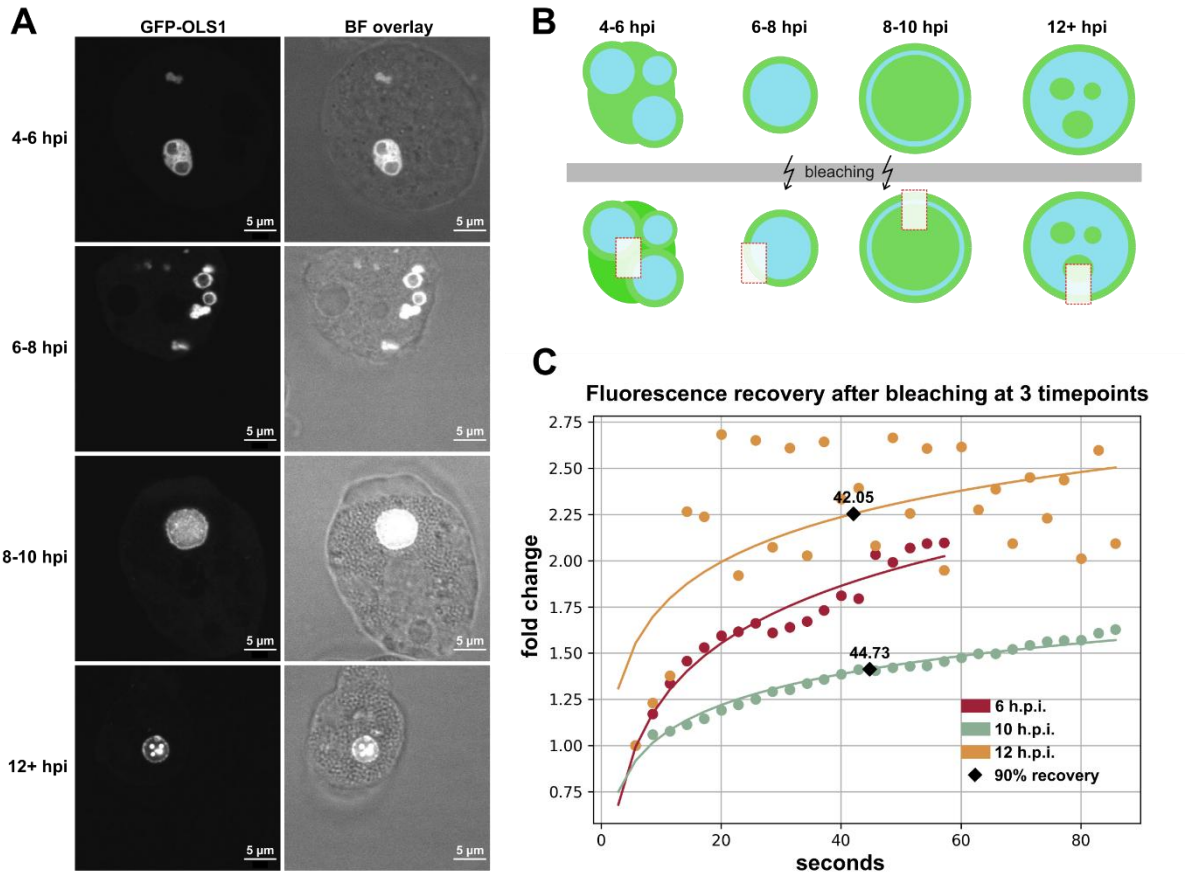

Figure 5: Comparison of protein localization and recovery speed at different timepoints *(**A**) Localization of GFP tagged OLS1 over the course of a* Mimivirus *infection. We observe a change in localization from predominantly outside the factory at early and intermediate timepoints to both inside and outside the factory at late stages of infection. (**B**) Schematic drawing of the different stages observed and where bleaching was applied. It is important to note that not all scans were obtained at corresponding locations to the ones indicated but these show the majority. (**C**) Fluorescence data obtained from bleaching the samples. The scatter plot shows the mean values while the line is a calculated regression approximating logarithmic growth. In black points where 90% of the maximum fluorescence was reached are indicated. This measurement is used to compare diffusion speed.*

2.3.2 Changes in biophysical properties

Understanding the biophysical properties of condensates is a crucial part of understanding changes in the progression of their function. The fluidity of a condensate influences the diffusion speed and therefore influences the speed at which reactions may take place as well as the general mobility of molecules. We have characterized different stages of outer layer condensate behaviour through the localization of its scaffold protein showing 4 distinctly different stages throughout the infection. To understand whether these 4 stages behave similarly, in collaboration with Hugo Bisio, we performed fluorescence recovery after photo-bleaching assays on live cells. For these assays a certain area of the condensate was bleached with a laser and then a time scan was acquired which showed how much fluorescence was recovered after a given amount of time and when recovery plateaued. To compare the fluidity of the condensates we compare how fast the curve plateaus. This depends on the speed of diffusion which changes depending on how fluid the condensate is. It is however important to note that changes in the recovery speed can also indicate binding of the OLS1 to other molecules

making a larger complex that moves more slowly. Further experiments are required to investigate the cause of differences observed in this assay.

Our results show differences in the recovery rates at different timepoints that are most pronounced at 10 h.p.i. compared to other timepoints (Fig. 5C). Early viral factories of up to 5 h.p.i. could not be measured due to rapid movement of the amoebae. The data acquired at 6 h.p.i. was excluded from formal analysis since we only acquired data up to roughly 60 seconds post -bleach while 10 h.p.i. and 12 h.p.i. were scanned for over 80 seconds. The preliminary data of 6 h.p.i. however shows similar behaviour of this timepoint to 12 h.p.i.. To compare how fast the curves reach a plateau, we calculated the points where they reach 90% of the maximum fluorescence. At 12 h.p.i. this was reached after 42.05 seconds while 10 h.p.i. reached 90% after 44.73 seconds (Fig. 5C). Further analysis and a larger sample size will be necessary to determine whether this difference is statistically significant.

Measuring fluorescence recovery after photo-bleaching (FRAP) we can also compare the mobile fraction of proteins in the condensate. This term refers to the proteins free to diffuse and can be measured by the height at which the curve reaches a plateau. The more proteins can diffuse the more fluorescence can be recovered and the higher the curve reaches a plateau. We observe a difference in the mobile fraction that is again most pronounced at 10 h.p.i. compared to other timepoints. The data was normalized against the fluorescence of the regions outside the bleached area to account for overall loss of fluorescence caused by both bleaching a significant part of the population of fluorescent proteins as well as general bleaching caused by the image acquisition. Additionally, we performed a baseline normalization to have the same starting values for each curve facilitating the comparison of relative fluorescence recovery. Our analysis shows the largest mobile fraction at 6 h.p.i.. This timepoint recovers 77% of fluorescence compared to pre-bleach fluorescence. Late timepoints show lower mobile fractions with the lowest being 54% at 10 h.p.i. and 66% at 12 h.p.i. This lower mobile fraction could be taken as an indication of the OLS1 being immobilized by interaction partners but could also indicate substantial hardening of the structure and should therefore be interpreted with care. The data currently available can only be used to characterise differences and not underlying mechanisms.

2.4 Outer layer sub-compartments have different biophysical properties

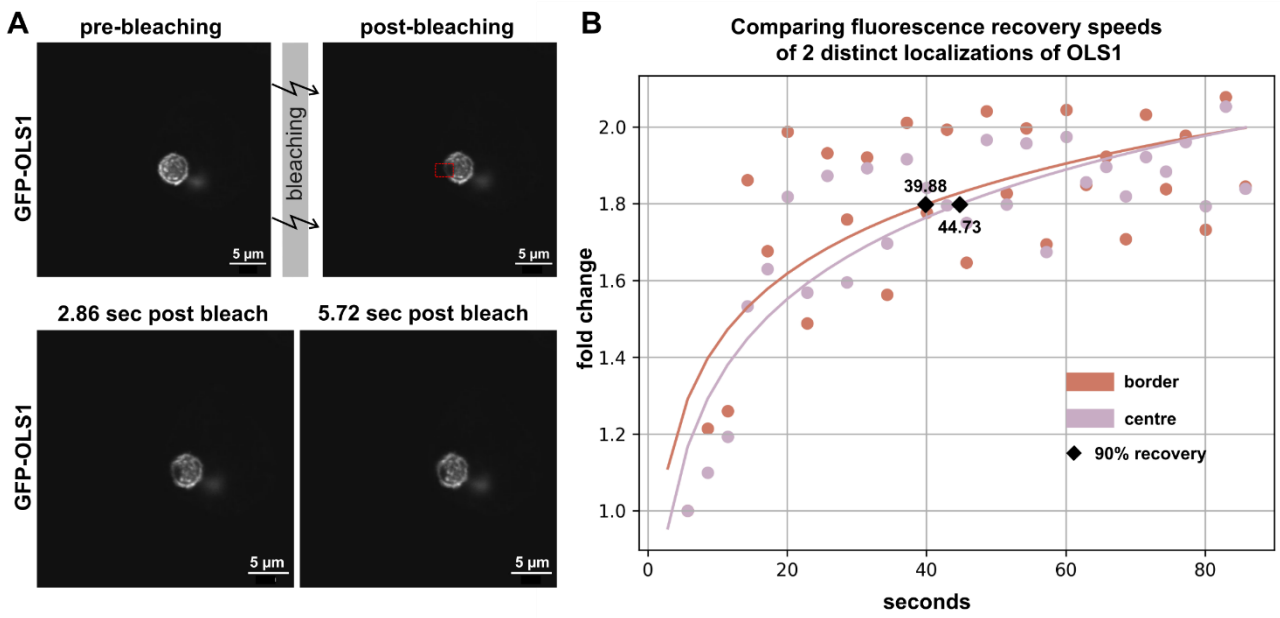

Figure 6: Comparison of fluorescence recovery rates of different localizations of the outer layer at late-stage infection *(**A**) shows images of a viral factory at 10 h.p.i. before and after bleaching showing rapid recovery of fluorescence around the factory already after 5.72 seconds while the center remains bleached. (**B**) shows fluorescence data obtained from bleaching the samples. The scatter plot shows the mean values while the line is a calculated regression approximating logarithmic growth. In black points where 90% of the maximum fluorescence was reached are indicated. This measurement is used to compare diffusion speed.*

Our observations show that the outer layer of the Mimivirus viral factory undergoes biophysical changes over the course of an infection that temporally correlate with changes in localization of the condensate. The spatial distribution of OLS1 goes from solely outside the factory to both inside and outside the factory. This change appears to happen at the same time as we observe changes in fluorescence recovery rates. Therefore, we further investigated whether there is a difference in recovery rates between the different sub-compartments. To this end we compared the recovery of the border (i.e. ring-like signal) with the center of the factory.

We observe a visually clear difference in fluorescence recovery speed between the border and the central sub-compartments of the outer layer condensate (Fig.6A). The contrast is most pronounced at 10 h.p.i., which is consistent with the results described above. Both data sets (border and center) contain data from 10 h.p.i. and 12 h.p.i. only. At 6 h.p.i. OLS1 does not localize in the center thus comparison between central and border signal cannot be made at this timepoint and was therefore excluded.

Our results show that the border region recovers after 39.88 seconds while the center only recovers after 44.73 seconds. This shows identical recovery rates of the center and 10 h.p.i. as described above which may be due to the large fraction of area the central part of the outer layer takes up at that timepoint. At 10 h.p.i. each region selected for bleaching

will inevitably be dominated by the central part of the outer layer due to its distribution at that timepoint (Fig. 5B) explaining the identical recovery rates. Comparing the results obtained from comparing the border to the center to the results of 12 h.p.i. (Fig. 5C) shows that overall, this timepoint shows a mixture of the rates consistent with the distribution of the sub-compartments (Fig. 5B). Further analysis will show whether the center at different timepoints and the border at different timepoints show variations in fluorescence recovery speed. This will however require a larger sampling size for each.

Comparing the border and the center we see that they recover to the same amount of final fluorescence. The starting fluorescence before bleaching however is different which gives us a mobile fraction of 48% for the border and 69% for the center. It is worth noting that the small movements that we were not able to correct during image processing affected the data recovery especially for small regions like the border potentially influencing the captured mobile fraction.

These results suggest that at 10 h.p.i. the outer layer sub-compartmentalizes leading to 2 compartments with distinctly different biophysical properties and localizations. Whether these two compartments are formed earlier and separate at late stages of infection or the sub-compartmentalization is introduced only at this stage remains to be investigated

2.5 mRNA colocalizes with the outer layer scaffold 1

The outer layer of the viral factory has previously been suggested to be involved in translation. Rigou et al.. show in their study that ribosomes co-precipitate with OLS1 and the eukaryotic translation initiation factor eIF4e localized at the outer layer as well[98]. This is consistent with our data showing translation at the periphery of the viral factory (Fig. 2).

Our results further suggest involvement of the outer layer in transcription. Signal distributions of mRNA (Fig. 1) and OLS1 (Fig. 5) at late stages of infection show striking similarities. Previous data showing distinct transcription sites adjacent to early viral factories suggest transcription may take place in the outer layer during early infection stages[99]. Combined with our data of late infection stages this indicates that the outer layer may be involved in maintaining transcription sites throughout the infection.

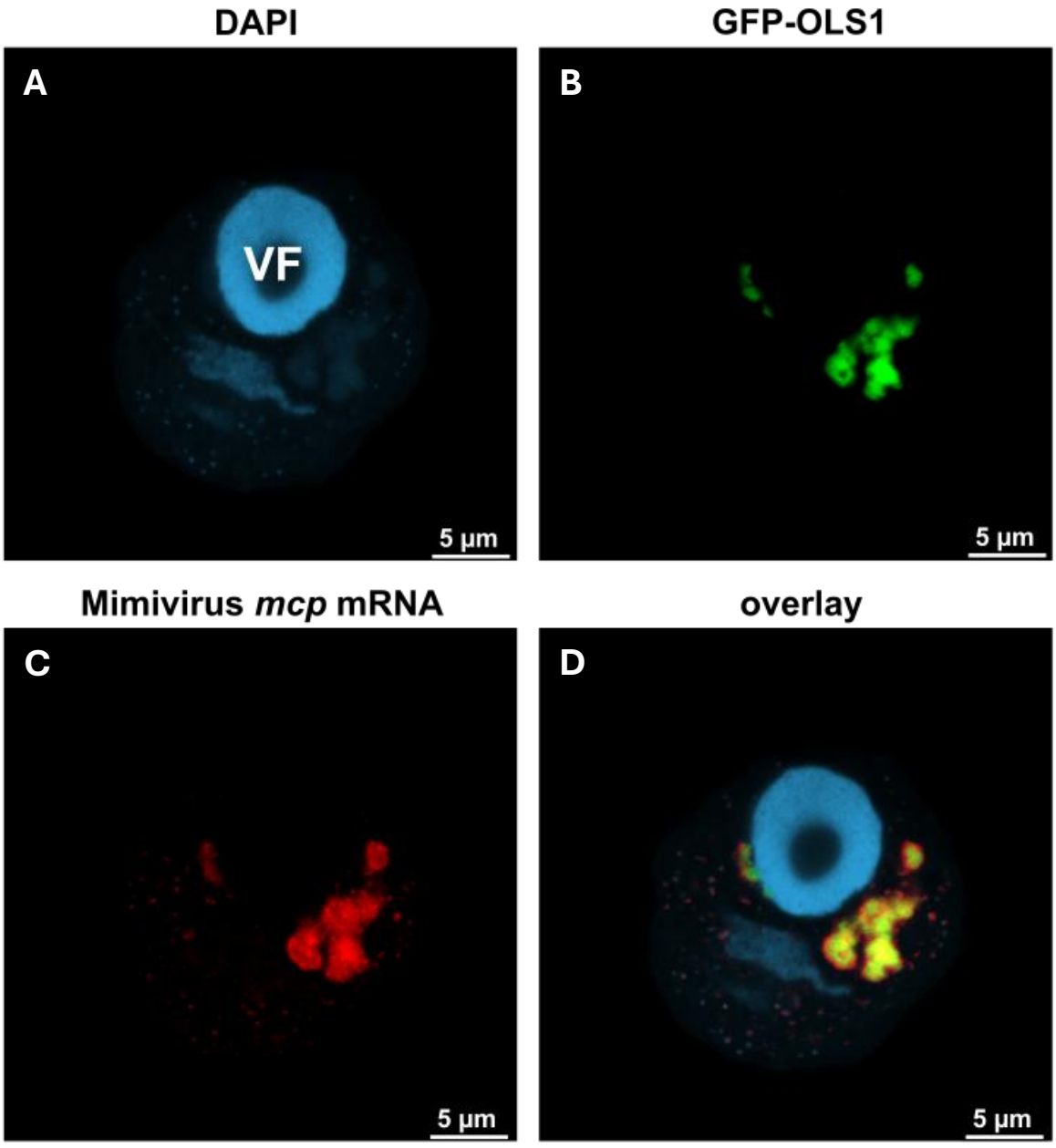

Figure 7: Colocalization of Mimivirus* mcp *mRNA with GFP-OLS1 aggregates. *The cells were infected with Mimivirus at MOI 5 and sampled after 13 hours of infection. Subsequently mRNA FISH was performed, and they were imaged using a confocal laser scanning microscope. (**A**) shows the viral factory stained by DAPI (light blue). In (**B**) we see the GFP-tagges OLS1in green and (**C**) shows viral mRNA visualized using smFISH in red. The overlay in (**D**) shows clear colocalization of viral mRNA and OLS1.*

To test this hypothesis, we used mRNA FISH on GFP-OLS1 overexpressing cells. Due to technical issues, we were only able to image the cells at 13 h.p.i.. The timing of infection the infection cycle can differ per experiment, depending on the cell batch, the temperature, medium, etc. In this case, many cells were lyzed and the viral factory had started to disintegrate, rendering the results of little biological significance. The overexpressed GFP-tagged OLS1 is known to form condensate like structures throughout the cell in uninfected cells as well as early stages of infection. We observe similar structures at 13 h.p.i. with some of the protein still localizing around the factory and large parts aggregating in random sites within the cell. These structures bear no biological

significance but are created by OLS1 as a result of its phase separating properties. In this preliminary data we observe mRNA localizing to these structures suggesting a strong association of mRNA with OLS1 formed condensates (Fig. 7).

2.6 MOI influences number of transcription sites in late-stage viral factories

To investigate whether the discrete mRNA spots we observe at late stages of infection in the mature viral factory are preserved from the initial sites of transcription initiation of each virus we followed the course of a Mimivirus infection with an increasing multiplicity of infection (MOI: the number of viral particles per cell).

Consistent with Mutsafi et al.[100], we observe that with an increasing MOI, a higher number of eVFs are formed within each cell (Fig. 8 and B at 4 h.p.i; *Spearman's rho* = 0.783, *P*-value < 2.2e-16, *S* = 293682, see also Fig. S1). This increase is significant at each MOI step (Fig. 8A and B at 4 h.p.i and Table S2). We use DAPI staining to count early viral factories at 4 h.p.i. which tells us how many virions were able to establish an infection. At 14 h.p.i. we count the number of distinct viral mRNA sites present inside the mature viral factory. Also, here, we observe that there is a positive correlation between the MOI and the number of distinct viral mRNA spots present in the fused VFs (Fig. 8B at 14 h.p.i; *Spearman's rho* = 0.749, *P*-value < 2.2e-16, *S* = 260134). The increase in the counted number of mRNA spots is significant at most steps (Fig. 8A and B; Table S2) except for the first (from MOI 0.5 to MOI 2). When comparing the counted eVFs and the distinct mRNA spots, there is no significant difference at most steps, except for MOI 2 (Fig. 8B; Table S2). These results suggest that the transcription sites established at the remnant of the viral core are conserved throughout the infection even after fusion of the early viral factories into one[101]. Each early viral factory contributes one transcription site. The progression of transcription localization throughout the full infectious cycle remains to be investigated.

Our previous results show association of mRNA to the outer layer condensate, and the distribution of this condensate exhibits the same sites within the factory that we observe using mRNA FISH. This strongly suggests that liquid-liquid phase separation and specifically the outer layer may be responsible for the maintenance of these sites from the very beginning of the infection. This may be further evidence for two potential sub-compartments of the outer layer. One for transcription, one for translation. Regulating transcription and translation in this manner may allow the virus to transport mRNAs quickly and efficiently while ensuring proper processing of mRNAs prior to translation. It would also make it possible for the virus to respond quickly and flexibly to environmental changes.

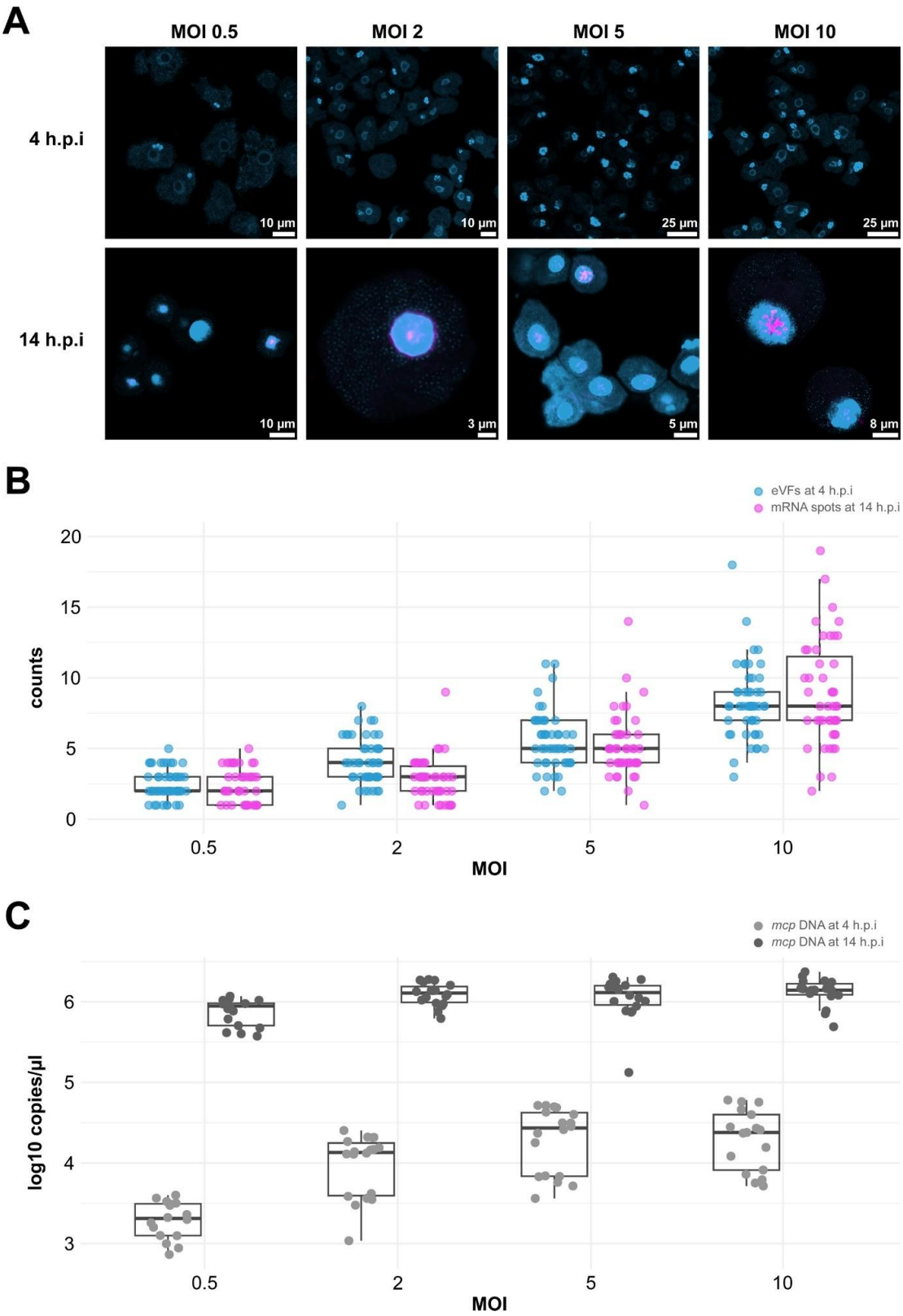

Figure 8: The original viral cores possibly serve separate transcription sites within the fused mature viral factory. *(**A**) DAPI staining (light blue) and Mimivirus mcp mRNA signal (magenta) of amoeba cells infected with different MOIs at 4 and 14 h.p.i. The Mimivirus mcp mRNA signal cannot be observed at 4 h.p.i as expression levels are undetectable at this time point. (**B**) The number of early viral factories counted at 4 h.p.i, and the number of distinct mRNA sites counted at 14 h.p.i after infection with different MOIs. Please note that only infected cells were considered for counting eVFs and mRNA spots. Therefore, the MOI 0.5 and MOI 2 appear inflated compared to the actual MOI used. (**C**) The viral copy number was measured by digital PCR at 4 h.p.i and 14 h.p.i. This image is part of already published work from the defendant [https://doi.org/10.1128/jvi.00554-25]*

3 Discussion

The results presented in this thesis provide novel insights into the architecture of the Mimivirus viral factory throughout the infection as well as the spatial organization of transcription and translation in late-stage infection. We further introduce protocols specifically developed to study giant virus infection which can be used to characterize single as well as co-infections (Fig. S3) of different viruses.

We provide evidence for spatial separation of transcription and translation at late stages of Mimivirus infection in amoeba host cells. We further provide preliminary results suggesting that the outer layer of the Mimivirus factory may be responsible for spatial organization of transcription and translation throughout the infection. Transcription is shown to take place in distinct sites, the number of which depends on the number of viral particles that establish an infection. This suggests these sites may be maintained throughout the entire infectious cycle, likely by liquid-liquid phase separation of the outer layer. We further provide evidence that translation takes place at the periphery of the viral factory likely also in the outer layer. We observe different localizations of both mRNA and the outer layer at late stages of infection (6+ h.p.i.) that correlate with changes in the observed diffusion behaviour of OLS1. Using FRAP we identified 10 h.p.i. as a timepoint of significant biophysical and structural changes of the viral factory.

The data presented in this thesis shows architectural changes of the viral factory beyond the fusion of early factories. We provide evidence for different “stages” of the mature viral factory. After fusion the outer layer of the viral factory remains around the factory until it migrates inward at 10 h.p.i. where it proceeds to condense into distinct sites in which transcription takes place. This splits the outer layer into two spatially separate sub-compartments. Furthermore, this change affects the architecture of the viral factory which is relevant to consider when studying the infection.

We hypothesize that the changes in localization and fluorescence recovery rate described in this thesis may be modulated via post translational modifications. Both the OLS1 and ILS1 have intrinsically disordered regions that can be modified which would allow the virus to control the shifts we observed easily and efficiently.

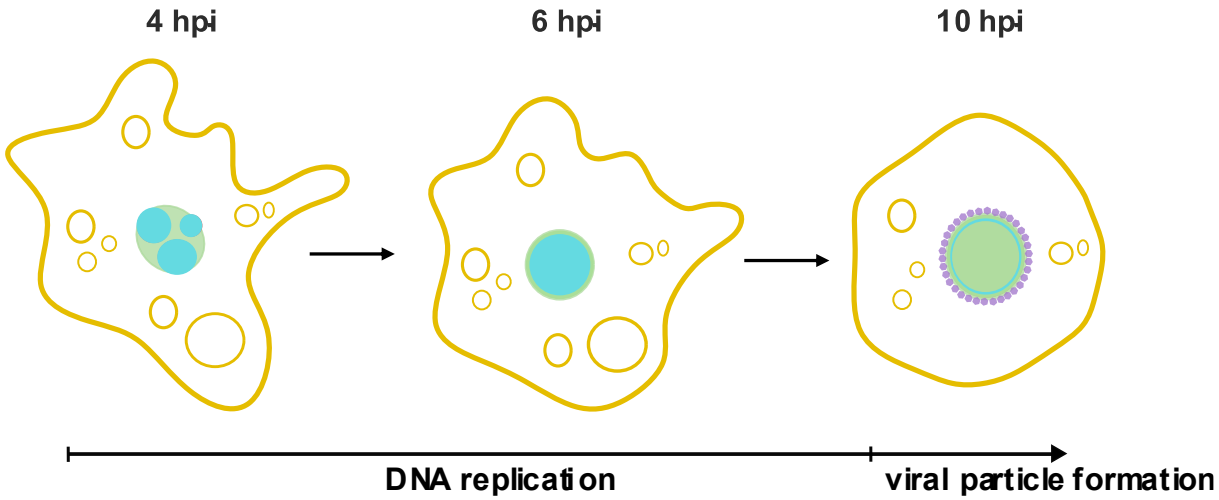

Figure 9: Schematic drawing showing the progression of the viral factory and the proposed "switch in purpose". *We propose that after 10 h.p.i. the purpose of the viral factory changes from DNA replication to viral particle formation. This is depicted as changes in the spatial distribution of the outer layer and viral DNA in the viral factory. Viral DNA is represented in blue, the outer layer in green, and viral particles are shown in purple.*

According to our observations 10 h.p.i. appears to be a key timepoint signifying a switch for the changes in localization as well as biophysical behaviour of the viral factory. This timepoint is typically when we start observing viral particles budding from the viral factory indicating an important timepoint during the infection. We hypothesize that there is a "switch in purpose" of the viral factory at that time of the infection moving from predominantly DNA replication to viral particle production. Whether this switch is what causes the changes in condensate behaviour and spatial distribution or vice versa remains to be investigated.

The results presented in this thesis provide a first glance inside the viral factory. We show where transcription and translation occur and provide a likely mechanistic explanation of their spatial separation. This spatial separation of the two processes bears a striking resemblance to the compartmentalization in eukaryotes showing a similarity on a functional level of the nucleus and the viral factory. Both the nucleus and the mature viral factory utilize liquid-liquid phase separation to efficiently orchestrate transcription within a very densely packed environment. The mRNA is then transported outside of the structure where it is translated by membrane associated ribosomes. This is evidence for both functional and architectural similarities between the nucleus and the late-stage viral factory of Mimivirus. Studies investigating transcription localization at early timepoints however show transcription taking place in distinct sites adjacent to early viral factories but not inside. As we have shown that both transcription and translation likely take place within the outer layer this result is consistent with the outer layer only localizing around the viral factory at corresponding timepoints. That however potentially constitutes a fundamentally different spatial organization of these two processes likely resembling a more prokaryote-like distribution.

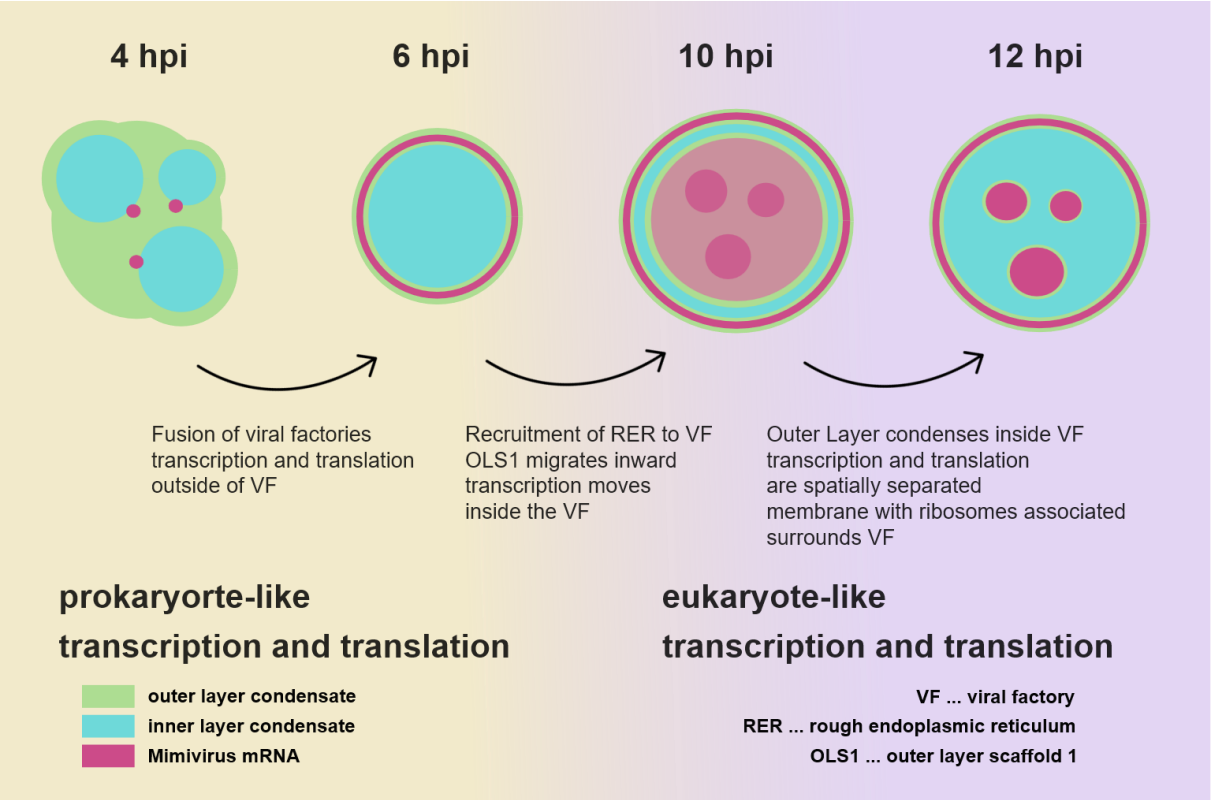

Figure 10: Schematic drawing of the proposed switch from a prokaryote-like to a eukaryote-like transcription and translation spatial organization.
Throughout the infection, mRNA localization (depicted in pink) changes from distinct sites adjacent to early viral factories (Mutsafi et al. 2010) to the periphery of the fused viral factory, to later condense inside the mature viral factory. Translation likely takes place in the outer layer through the entire infectious cycle. This implies that, in early stages of infection, transcription and translation occur in the same environment. However, later they become spatially separated, constituting a change from a prokaryote-like to a eukaryote-like system.

We therefore hypothesize that throughout the infection the mode of transcription and translation changes from prokaryote-like to eukaryote-like. We propose that during early stages of infection the transcription sites are within the outer layer of the viral factory and therefore in the same general space of translation occurring suggesting a lower level of compartmentalization and spatial segregation. As the infection progresses and we observe the previously described “switch” in the viral factory the mode of spatial organization of transcription and translation changes to a more eukaryote-like spatial separation.

4 Methods

4.1 Fluorescence recovery after photo-bleaching (FRAP)

4.1.1 Sample preparation

A. terricola Neff (ATCC 30010) expressing GFP-OLS1 were seeded in PYG with 30 mg/mL Geneticin with 100 µg/mL Ampicillin and 25 µg/mL Kanamycin in 12 well-plates (Thermofisher Scientific #140675) containing pre-prepared round Poly-L-Lys coated coverslips at approximately 10^5 cells/mL using 2 mL per well. The cells were left at 32°C overnight and then infected with Mimivirus using a high MOI (10+) to ensure all cells are infected.

4.1.2 Imaging

For imaging an Olympus IX81 inverted Confocal Laser Scanning Microscope was used with the 100x lens and the µManager Software. Laser intensity and Voltage were adjusted according to the sample before starting the experiment.

The coverslips were removed from the well, placed on a slide and mounted with nail polish. Laser intensity and Voltage were adjusted according to the sample before starting the experiment. To bleach 100% of the previously set laser intensity was used for 1.5 seconds. A defined area of 10 x 5 mm was used to select the region of interest. Regions were selected to obtain equal amounts of information on inner and outer regions of the viral factory although it is worth noting that the viral factory moved significantly during the process which led to difficulty controlling the placement of the region of interest. This was corrected for during analysis. After bleaching the cells were imaged at maximum speed (2,86 sec/scan) 30 times to make sure fluorescence recovery was captured.

4.1.3 Analysis

The obtained data was analyzed using Fiji. Cellular movement was corrected using a macro. To correct for overall bleaching of the cell the bleached area was cleared, and fluorescence intensity of the condensate was measured. Measurements of the bleached area were split into areas of the condensate e.g. outer ring and center to obtain separate data. This separation was achieved using the wand tool to segregate areas of similar fluorescence intensity neighbouring a starting point. All measurements were normalized against the first value and against the measurement of the whole condensate to correct for bleaching during scanning and sample specific intensity differences.

As mentioned above movements of the viral factory posed a problem in data extraction and scans were individually analyzed and compared with regards to viability of the data and fit of necessary corrections.

4.1.4 Remaining problems in data analysis and interpretation

Interpreting FRAP data and comparing it quantitatively comes with a unique set of difficulties. Some of the difficulties stem from live imaging as the factories move and twist and turn during scanning making data extraction difficult especially for small regions like the border. This can distort the data very easily.

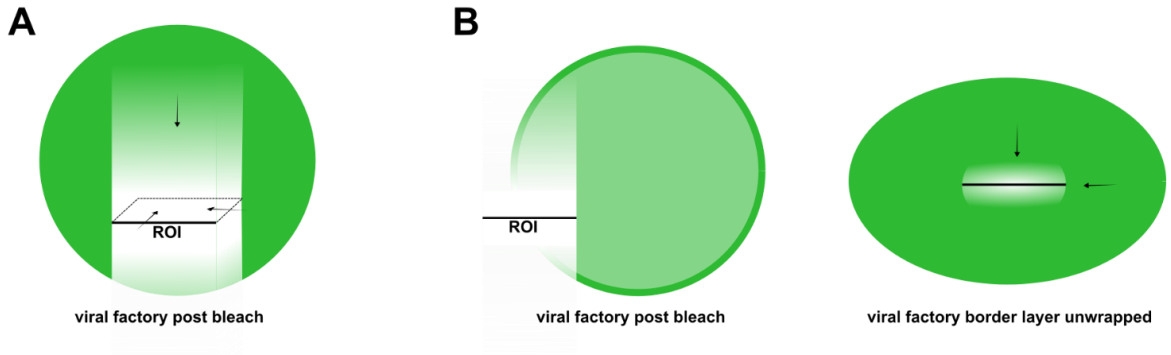

Figure 11: Schematic of 2 main problems interpreting FRAP data *(**A**) shows a schematic drawing of what the central part of the mature viral factory looks like after bleaching. The green represents GFP tagged OLS1 and the rectangle represents the region selected for bleaching. Each arrow shows a possible direction from which molecules can diffuse into the region of interest to contribute to fluorescence recovery. (**B**) shows a two-dimensional view of the viral factory post bleach focussing on the layer surrounding the factory. The layer is "unwrapped" to visualize how the bleaching affected the structure. Again, the arrows indicate possible directions molecules can diffuse in.*

Another consideration that is important is to take into account the "pool of available proteins". We are bleaching a certain region of the condensate in a layer of interest; the laser however penetrates much further into the sample along the z axis than just the layer we selected as depicted in Fig. 11A. That means all proteins in the white column are bleached and therefore eliminated from the pool of proteins that can contribute to fluorescence recovery.
To understand how and if that influences our sample, we performed a z stack on a fixed sample that was bleached like it would be for FRAP. This experiment showed that the laser does not penetrate the entire factory. As this was performed on late stages of infection the factory was at its largest stage suggesting that at early stages of infection the laser would penetrate the entire condensate. These considerations are important to understand how many degrees of freedom the molecules have to diffuse back into our region of interest.

This implicates how we compare not only the timepoints but mainly the center and the border of the condensate. The center while it varies in size can be considered spherical. At late stages of infection, it must be treated as 3 dimensional adding a degree of freedom to diffusion that is not present in the border. The border on the other hand can be considered two-dimensional at all times and can be compared to a membrane. Unwrapping the layer to visualize this would leave us with a thin layer of proteins with a bleached hole in the middle. One thing we cannot take into account as we do not have enough knowledge as of now is whether proteins from the center can diffuse into the layer and vice versa. The data collected so far suggests that spots within the factory as

observed at 12 h.p.i. can recover after being fully bleached but whether the proteins come from other spots or from the outer layer we cannot say.

It is further relevant to note that while FRAP data is useful to observe changes in behaviour of biomolecular condensates this method alone does not allow us to draw conclusions on the mechanism causing the change. A slower recovery rate observed by FRAP could therefore indicate either a hardening of the condensate or interactions of the observed protein with larger molecules. This makes FRAP data difficult to interpret without complementing methods.

4.2 Fluorescent stainings

The following methods are part of already published work from the defendant [https://doi.org/10.1128/jvi.00554-25]

4.2.1 Sample preparation

A. terricola Neff (ATCC 30010) cells were seeded in a 24-well plate (Thermo Fischer Scientific #142475) in Peptone-Yeast Extract-Glucose medium (PYG: ATCC Medium 712) at a concentration of 10^5 cells/mL, and 1 mL per well. Subsequently, the cells were left to attach at 25°C for 30 min. *Acanthamoeba polyphaga mimivirus* was added at an MOI of 1, and the plates were centrifuged at 1,000 × *g* at room temperature (RT) for 30 min to synchronize the infection. To minimize the possibility of re-infections, the medium was exchanged after centrifugation. For all experiments, the cells were incubated in an incubator at 25°C.

After the desired hours post-infection (h.p.i), the cells were detached by scraping, and the cell suspension of each well (~1 mL) was collected in a 1.5 mL Eppendorf tube. The tubes were centrifuged at 5,000 × *g* at RT for 5 min, 800 µL of the supernatant was removed, and the pellet was resuspended in the remaining 200 µL through vortexing. Then, 50 µL of each cell suspension was added to a well of a microscope slide (Marienfeld #1216690), and the cells were left to attach for 1 h at RT. The supernatant was removed from each well, and the samples were fixed with 20 µL 4% formaldehyde for 10 min at RT. Subsequently, the formaldehyde was removed, and the slides were washed with 40 µL of RNAse-free water. The cells were permeabilized with 40 µL of 70% ethanol for 1 h at 4°C. After permeabilization, 70% ethanol was removed from each well and left to evaporate further. To test whether the probes bind to RNA and not to DNA, an RNase treatment was performed by adding a final concentration of 10 µg/mL RNase A (Thermo Scientific #EN0531) for 30 min at 37°C to the slides after permeabilization.

The number of cells that attach to the microscope slide is higher at the early time points (4 and 6 h.p.i.) compared to the late time points (14 and 20 h.p.i.), as the cells tend to round up at these later time points. Therefore, to harvest a sufficient number of infected cells, we initiate our experiments with a high number of cells and treat them with great care to ensure minimal cell loss before fixation.

4.2.2 Fluorescent noncanonical amino acid tagging

For performing FUNCAT, the amino acid homopropargylglycine (HPG) was added to the amoeba culture at least 30 min before sampling at a concentration of 50 µM. To dehydrate and permeabilize the samples they were incubated in 40 µl 70% Ethanol for at least 30 min at 4°C. The Ethanol was removed by evaporation and washing with 40 µl ice-cold PBS. In the meantime, the dye mix (1.25 µL of 20 mM $CuSO_4$, 1.25 µL of 100 mM THPTA, and 0.3 µL 5 mM Cy3-azide) was prepared and incubated in the dark at RT for 3 min. Then, the dye mix was gently mixed with a freshly prepared mix of 221 µL Page's Amoeba Saline buffer (PAS: ATCC medium 1323), 12.5 µL of 100 mM sodium ascorbate, and 12.5 µL of 100 mM

aminoguanidine hydrochloride. Each sample was covered in 10 µl of the final mix and incubated 30 min in the dark. After the incubation they were washed using 40 µl 1X PBS.

4.2.3 Single-molecule messenger RNA fluorescence *in situ* hybridization

After permeabilization, and optionally the FUNCAT click reaction, the slide was air-dried and 10 µL of smFISH Hybridization Buffer ([102]; 20% deionized formamide, 1 mg/mL *E. coli* tRNA, 2× SSC, 0.2 mg/mL BSA, 2 mM ribonucleoside-vanadyl complex, 100 mg/mL dextran sulphate, and nuclease-free water) containing 437.5 nM of probe working solution was added to each well of the slide. For hybridization, the slide was incubated in a moist chamber in the dark at 37°C overnight (~20 h). The smFISH Hybridization Buffer was removed, and the slide was transferred into a 50 mL tube containing Wash Buffer (2× SSC, nuclease-free water) and incubated in a water bath at 39°C for 10 min. After washing, the slides were dipped into ice-cold Milli-Q water and air-dried. The different conditions tested for setting up the smFISH protocol and obtaining an optimal signal are displayed in Table 2.

Step in protocol	Concentrations and/or conditions tested		
	smFISH	**rRNA FISH**	**Stellaris RNA FISH**
Sample preparation			
Fixation	4% formaldehyde: 1 h, 30 min, 10 min at RT		
Permeabilization	70% ethanol: 1 h and 30 min at 4°C; proteinase K: 1-10 min at RT		
Hybridization			
Ingredients (final concentration)	1.25, 2.5, 3.75, 4.375, and 5 ng/µL probe mix		
	0%, 10%, 15%, 20%, 25%, 30%, 35%, 40%, and 50% formamide		
	1 mg/mL *E. coli* tRNA	900 mM NaCl	Stellaris hybridization buffer
	2× SSC	20 mM Tris/HCl	
	0.2 mg/mL BSA	0.01% SDS	
	2 mM ribonucleoside-vanadyl complex		
	100 mg/mL dextran sulfate		
	Nuclease-free water		
Temperature	32°C, 37°C, 42°C		
Time	5 h, 17 h, 20 h		
Post-hybridization			
Initial wash	20% formamide, 2× SSC, 15 min at 37°C and 39°C		Wash Buffer A
Final wash	Ice-cold Milli-Q water		Wash Buffer B

Table 1: Conditions tested for performing smFISH protocol

Different percentages of formamide, ranging from 0% to 50%, were tested in the hybridization buffer. These formamide series show that although 10% formamide already gives a crisp signal (Fig. S2), the optimal formamide concentration for this probe mix and target sequence is 20%, as this concentration leads to less variability in fluorescent signals between experiments. As a negative control, the cells were treated with RNase A before fixation. No signal was observed when performing the same protocol on RNase-treated cells (Fig. 13).

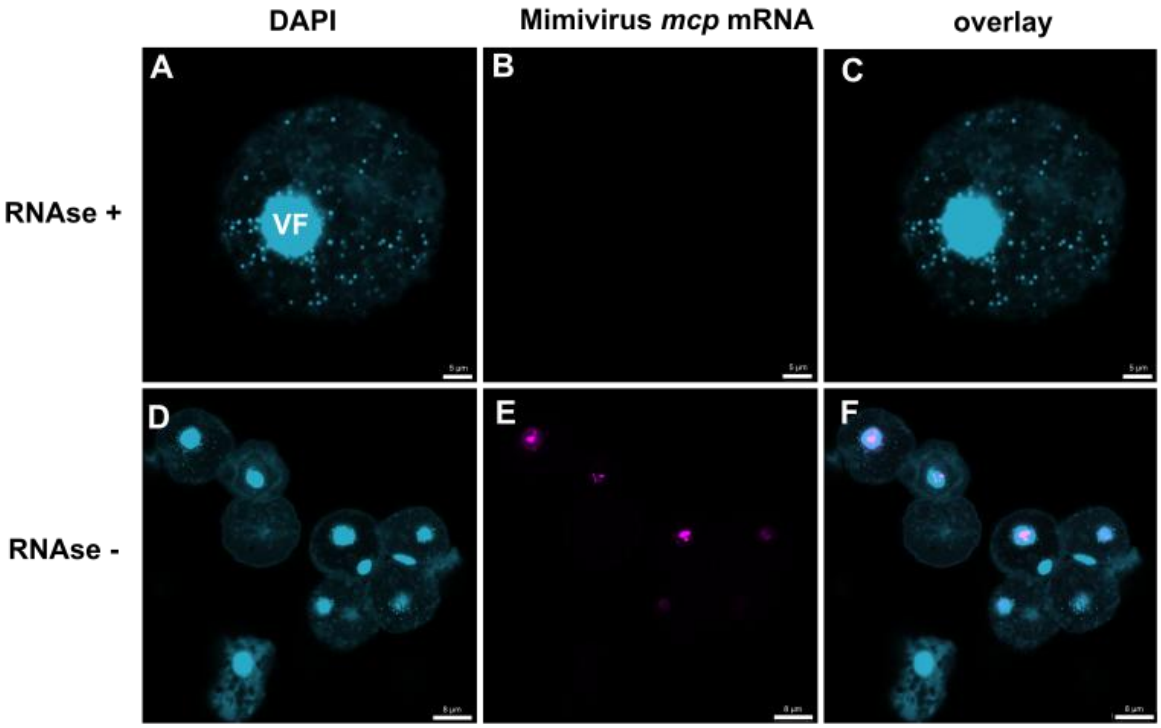

Figure 12: smFISH performed on cells treated with RNAse compared to untreated cells. *To confirm that the probes bind to RNA and not DNA, the cells were treated with RNAse A (A, B, C) and compared to the untreated condition (D, E, F). DAPI staining (light blue), Mimivirus* mcp *mRNA signal (magenta), and the overlay of infected amoeba cells.*

4.2.3.1 Probe design

Custom Stellaris FISH Probes were designed against the *Acanthamoeba polyphaga mimivirus* (GenBank: HQ336222.2) major capsid protein (*mcp*) gene by utilizing the Stellaris RNA FISH Probe Designer (Biosearch Technologies, Inc., Petaluma, CA) available online at https://www.biosearchtech.com/support/tools/design-software/stellaris-probe-designer (Version 4.2; masking level = 2, oligo length = 20, minimum spacing = 2). To avoid potential off-target binding, we performed blastn[103] searches of the 68 possible probe sequences against the *Acanthamoeba terricola Neff* host genome (RefSeq: GCF_000313135.1) and other giant virus genomes (*Tupanvirus deep ocean*: MF405918.1, *Tupanvirus soda lake*: KY523104.1, *Marseillevirus sp*. strain Vienna: PP736097.1, *Acanthamoeba castellanii medusavirus* J1: AP018495.1). Out of the 68 sequences, we selected 35 probes for smFISH (Table S1). The probe sequences were hybridized with the Quasar 670. Stellaris RNA FISH Probe set labeled with (Biosearch Technologies, Inc.), following the manufacturer's instructions online at https://www.biosearchtech.com/support/resources/stellaris-rna-fish/stellaris-protocols.

4.2.4 Ribosomal RNA fluorescence *in situ* hybridization

For rRNA FISH, 10 µL of rRNA FISH Hybridization Buffer (900 mM NaCl, 20 mM Tris-HCl pH 8.0, 0.01% SDS, and 25% formamide) containing 5 µM of Euk516 probe (5'-GGAGGGCAAGTCTGGT-3'; labelled with the fluorophore Fluos) working solution was added to each well of the microscopy slide. Hybridization was performed in a moist chamber in the dark at 46°C for 1.5 h. Subsequently, slides were washed with a wash buffer (201 mM Tris-HCl pH 8.0, 50.25 mM EDTA, and 0.149 M NaCl) and kept in the wash buffer in a 50 mL tube at 48°C for 10 min. Then, the slides were dipped in ice-cold Milli-Q water and air-dried.

4.2.5 DiD staining

DiD (1,1'-dioctadecyl-3,3,3',3'-tetramethylindodicarbocyanine, 4-chlorobenzenesulfonate salt; Thermo Fischer Scientific #D7757) staining was performed after permeabilization. The staining solution (1 µM DiD in 96-100% Ethanol) was sonicated for 30 min. After this homogenization step, 3 µL of staining solution was added to each well of the microscope slide and incubated at 37°C for 20 min. After incubation, the wells were washed with 40 µL of PAS at RT for 5 min.

4.2.6 Imaging

After the smFISH, FUNCAT, rRNA FISH, and/or DiD staining, 4,6-diamidin-2-phenylindole (DAPI) (1 µg/mL) was added to the wells on the slides, incubated for 3 min, washed off with nuclease-free water, and air-dried. The slides were embedded in CitiFluor AF1 Mounting Medium (Electron Microscopy Sciences #17970-25) and imaged using a confocal laser-scanning microscope (Leica SP8).

4.3 MOI experiments

The following methods are part of already published work from the defendant [https://doi.org/10.1128/jvi.00554-25]

A. terricola Neff cells were infected with *A. polyphaga mimivirus* (as described above) using an MOI of 0.5, 2, 5, and 10. Each well from a 24-well plate was sampled at 4 and 14 h.p.i., and for each MOI and time point, at least five different replicates (wells) were used, and the experiment was repeated 3 times, giving a minimum of 15 data points per MOI and time point.

For each MOI, the samples were subjected to smFISH, DAPI staining, and confocal laser-scanning microscopy. To count the number of eVFs at 4 h.p.i, at least 50 infected cells were used per MOI. To count the number of distinct *mcp* mRNA spots at 14 h.p.i, at least 45 infected cells were used per MOI.

4.3.1 Digital polymerase chain reaction (dPCR)

For DNA extraction, the content of each well was collected in a 1.5 mL Eppendorf tube and centrifuged for 30 min at 13,000 × *g* at 10°C. The supernatant was replaced with 200 µL PAS, and the pellet was resuspended through vortexing. DNA was extracted using the DNeasy Blood & Tissue Kit (Qiagen #69506), adding 20 µL proteinase K and 200 µL Buffer AL and incubating at 56°C for 30 min at 400 rpm at the first steps. The DNA copy number of Mimivirus was quantified by performing digital PCR (dPCR) on the extracted DNA using the QIAcuity system and QIAcuity EG PCR Kit (Qiagen #250113). Primers targeting the *mcp* gene of Mimivirus (MCP_APolyphagaMimivirus_F:5'-TCGTTTTTACGAAACATGATGG-3'; MCP_ApolyphagaMimivirus_R: 5'-CGATGGTGATTTGGAACACA-3') were used as a proxy for measuring viral copy number.

4.4 Statistics and data visualizations

The data was visualized and processed using Python 3.11.0 with the libraries matplotlib, pandas, numpy and scipy. Figures were made using Inkscape v.1.3.2.

5 Supplementary information

Probe sequence (5'→3')	Position on gene	GC
aattggagtaaaccacctgc	4	45,00%
acatcttgagcaccataagc	28	45,00%
tgatcattggattaccggtt	54	40,00%
gtcgcctataaactacctta	81	40,00%
ctcaatggattctacggcga	110	50,00%
ccaagattacccccgaaaaa	133	45,00%
tctgcactagatttctttcc	157	40,00%
tcaacgtgaccgaaattagt	256	40,00%
gaagtaagttcaggtacgtc	436	45,00%
cagagtatatgaaggcttca	497	40,00%
gaccgttgttacgattgaaa	537	40,00%
acattgatcagcttgtctga	611	40,00%
ccagatttgaaggcatcact	640	45,00%
tctacgttcttcagtgtcaa	713	40,00%
cagattcttcaccagtgaat	777	40,00%
tacccaatttagttacccaa	858	35,00%
ttttcccaacaaaccggatc	907	45,00%
ggaaataaccccaatcgtca	975	45,00%
cattcataacctccaggttc	997	45,00%
acttctaccatcattacctt	1019	35,00%
aactgggttcttcagaagga	1086	45,00%
ccttgtttctcttgagaaga	1182	40,00%
cgactttatccttgagatcg	1206	45,00%
gtgtgaattcggatgattcc	1228	45,00%
gtaattttctctacttcagg	1276	35,00%
gatcgtgaagagtgagatca	1302	45,00%
gattaccagaaccgtcaata	1419	40,00%
tgaagttcagcttcatgagt	1441	40,00%
actgtgggattaacagtgtc	1507	45,00%
tctgggtgatttagtatgat	1529	35,00%
tgttcttcagggttaagagc	1573	45,00%
taagttgcgcggtatcgata	1623	45,00%
gtggttagtgaaatgttgga	1652	40,00%
ccgctaagcattctgagaac	1735	50,00%
attactgtacgctaatccgg	1760	45,00%

Table S1. *Selected probe sequences that target the mcp gene of Mimivirus.*

Groups compared		P value	W	Location difference	95% CI	
eVF MOI 0.5	eVF MOI 2	3,786E-07	545	-0,17613	-0,30101	-0,17606
eVF MOI 0.5	eVF MOI 5	5,248E-14	181	-0,36798	-0,42592	-0,30097
eVF MOI 0.5	eVF MOI 10	< 2.2e-16	23	-0,54411	-0,60211	-0,47707
eVF MOI 2	eVF MOI 5	6,919E-05	680	-0,14610	-0,22191	-0,07919
eVF MOI 2	eVF MOI 10	1,112E-13	179,5	-0,30107	-0,39790	-0,25522
eVF MOI 5	eVF MOI 10	8,795E-08	479,5	-0,17605	-0,22190	-0,12490
mRNA MOI 0.5	mRNA MOI 2	2,124E-01	895,0	-0,00003	-0,17609	0,00008
mRNA MOI 0.5	mRNA MOI 5	2,625E-10	211,5	-0,30106	-0,47712	-0,22188
mRNA MOI 0.5	mRNA MOI 10	1,615E-14	57,0	-0,54409	-0,69895	-0,47705
mRNA MOI 2	mRNA MOI 5	2,431E-09	336,5	-0,30102	-0,30108	-0,17612
mRNA MOI 2	mRNA MOI 10	1,099E-14	111,0	-0,47712	-0,57983	-0,39796
mRNA MOI 5	mRNA MOI 10	1,151E-07	382,5	-0,24303	-0,30110	-0,14617
eVF MOI 0.5	mRNA MOI 0.5	7,950E-01	1104,0	0,00001	-0,00006	0,12494
eVF MOI 2	mRNA MOI 2	1,503E-04	1786,5	0,17605	0,09690	0,22191
eVF MOI 5	mRNA MOI 5	1,803E-01	1302,5	0,05795	-0,00005	0,09695
eVF MOI 10	mRNA MOI 10	6,287E-01	1108,0	-0,00005	-0,07914	0,05797

***Table S2**. Wilcoxon rank sum tests for the counts of the early viral factories (eVFs) and mRNA spots.*

Groups compared		P value	W	Location difference	95% CI	
T4 MOI 0.5	T4 MOI 2	5,138E-06	23	-0,75024	-0,94278	-0,53776
T4 MOI 0.5	T4 MOI 5	3,630E-09	2	-1,06904	-1,27137	-0,76079
T4 MOI 0.5	T4 MOI 10	1,714E-09	0	-1,02749	-1,26296	-0,77792
T4 MOI 2	T4 MOI 5	9,631E-03	81	-0,30844	-0,52607	-0,12829
T4 MOI 2	T4 MOI 10	1,391E-02	79	-0,28497	-0,56440	-0,08203
T4 MOI 5	T4 MOI 10	9,870E-01	154	0,00178	-0,25051	0,26823
T14 MOI 0.5	T14 MOI 2	1,337E-04	43	-0,20669	-0,31916	-0,10264
T14 MOI 0.5	T14 MOI 5	3,824E-03	67	-0,21241	-0,30612	-0,09137
T14 MOI 0.5	T14 MOI 10	2,664E-05	34	-0,23291	-0,36819	-0,14712
T14 MOI 2	T14 MOI 5	9,626E-01	164	0,00313	-0,10086	0,11189
T14 MOI 2	T14 MOI 10	2,788E-01	127	-0,03906	-0,13259	0,06040
T14 MOI 5	T14 MOI 10	6,058E-01	145	-0,05116	-0,16913	0,05855
T4 MOI 0.5	T14 MOI 0.5	1,714E-09	0	-2,56336	-2,72101	-2,42597
T4 MOI 2	T14 MOI 2	2,204E-10	0	-1,98538	-2,32773	-1,86356
T4 MOI 5	T14 MOI 5	2,204E-10	0	-1,67702	-2,04092	-1,50514
T4 MOI 10	T14 MOI 10	4,408E-10	0	-1,77460	-2,06061	-1,58086

***Table S3.** Wilcoxon rank sum tests for the digital PCR data*

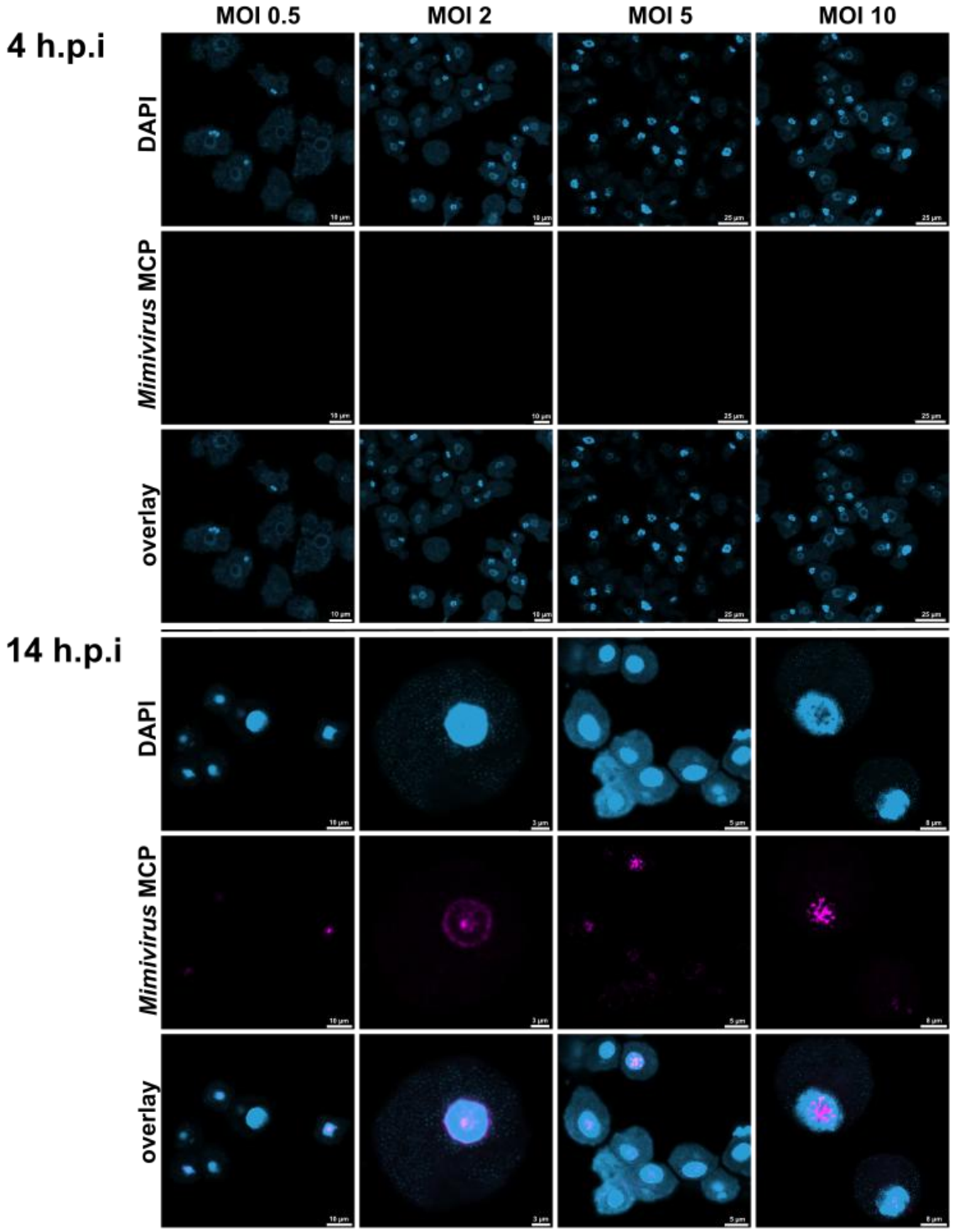

Figure S1: ***The full version of Fig. 8A****. DAPI staining (light blue) and Mimivirus* mcp *mRNA signal (magenta) of amoeba cells infected with different MOIs at 4 and 14 h.p.i. The Mimivirus* mcp *mRNA signal cannot be observed at 4 h.p.i as expression levels are undetectable at this time point. This image is part of the supplementary material of already published work from the defendant [https://doi.org/10.1128/jvi.00554-25].*

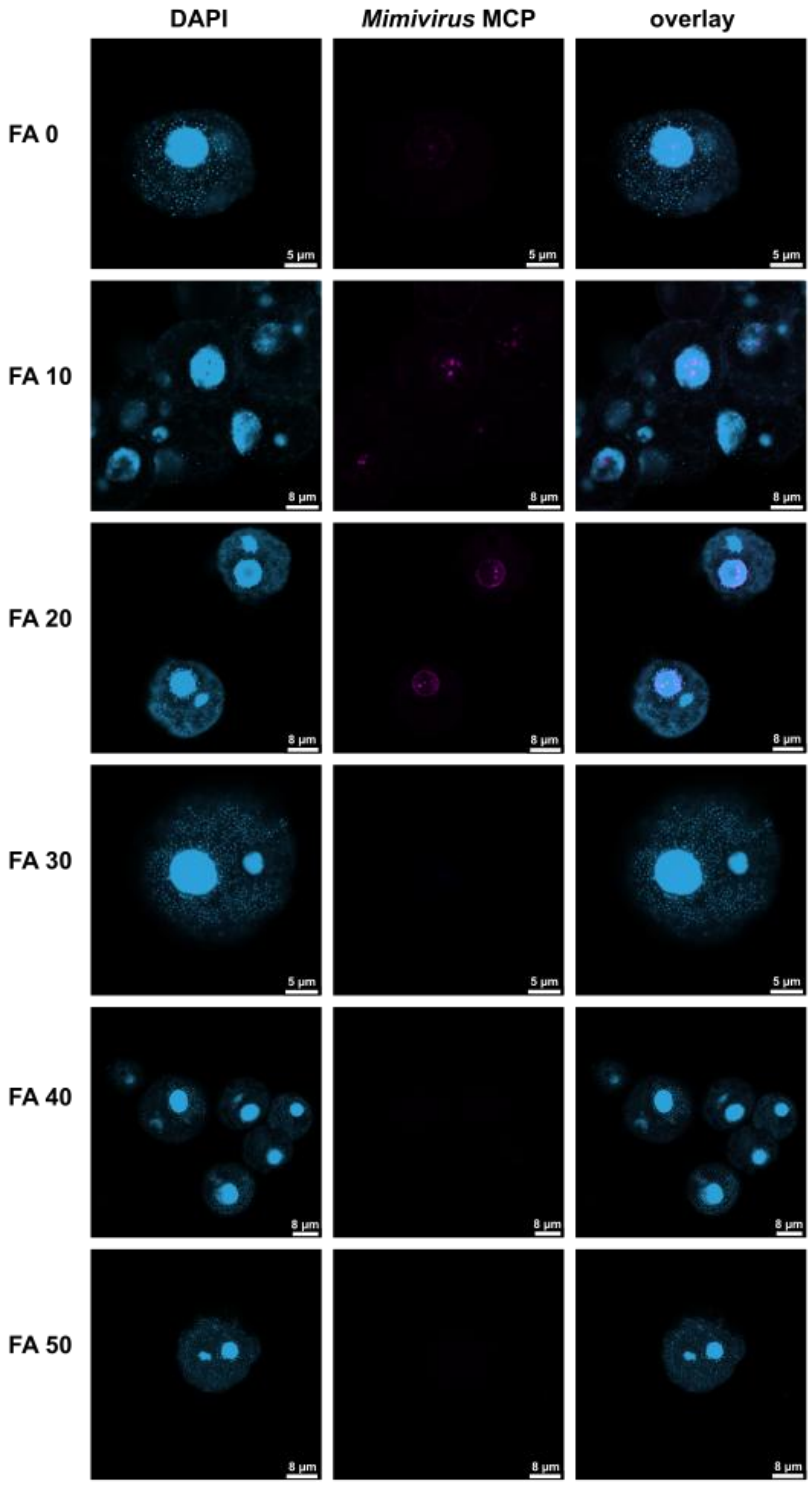

Figure S2: **smFISH using different Formamide concentrations.** *Different formamide (FA) concentrations (0-50%) in the hybridization buffer were used to determine the optimal concentration for the probe mix and target sequence. The first column is the signal of DAPI staining (light blue), the middle column is the Mimivirus* mcp *mRNA signal (magenta), and the third column is the overlay. This image is part of the supplementary material of already published work from the defendant [https://doi.org/10.1128/jvi.00554-25].*

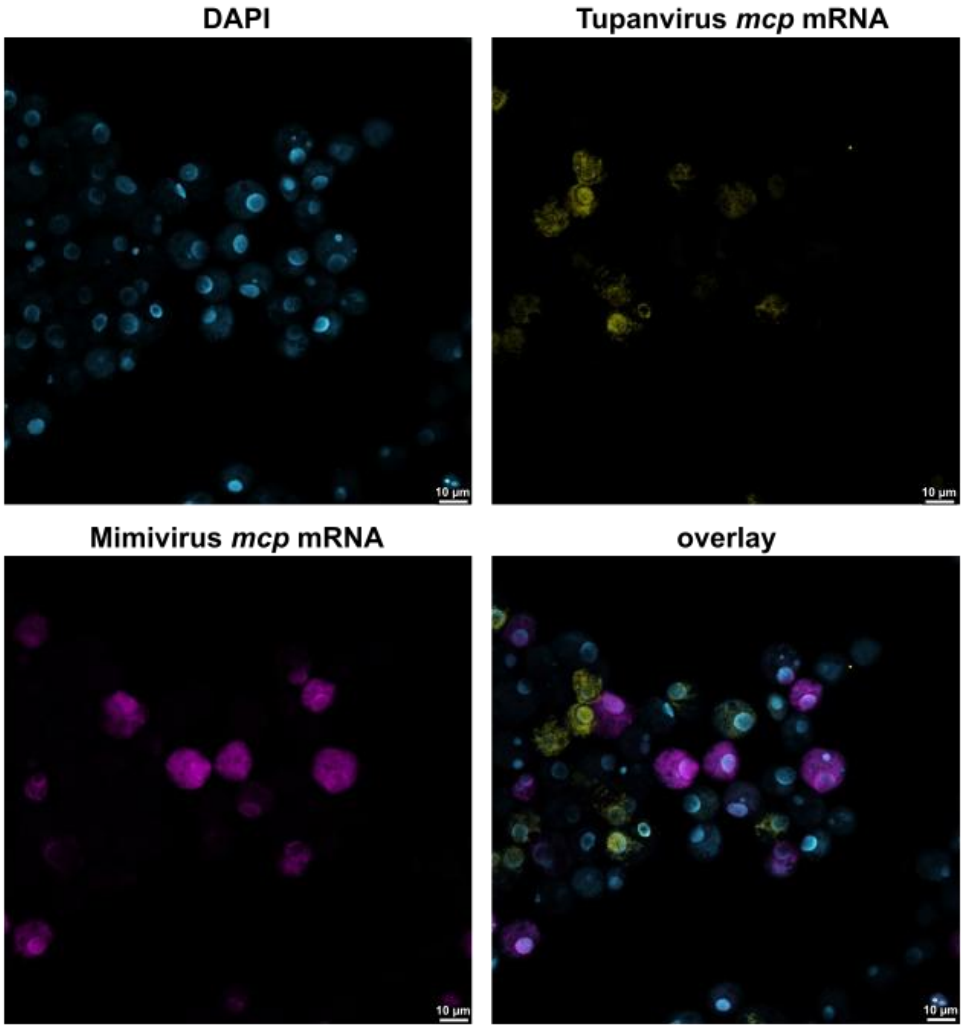

Figure S3: Distinguishing cells infected with different giant viruses using smFISH. *Our smFISH protocol can be used to visualize mRNA in different giant viruses and allows us to distinguish between cells infected by different viruses in the same population of cells*

[1] Lane N. 2011 Energetics and genetics across the prokaryote–eukaryote divide. *Biol. Direct* **6**, 35.
[2] Guigas G, Kalla C, Weiss M. 2007 The degree of macromolecular crowding in the cytoplasm and nucleoplasm of mammalian cells is conserved. *FEBS Lett*. **581**, 5094–5098
[3] Hudder A, Nathanson L, Deutscher MP. 2003 Organization of mammalian cytoplasm. *Mol. Cell Biol*.
[4] Kerfeld C a, Heinhorst S, Cannon GC. Bacterial microcompartments. Annu. Rev. Microbiol. 2010;64:391–408. doi: 10.1146/annurev.micro.112408.134211
[5] Vothknecht UC, Westhoff P. Biogenesis and origin of thylakoid membranes. Biochim. Biophys. Acta. 2001;1541:91–101. doi: 10.1016/s0167-4889(01)00153-7
[6] Lindsay M, Webb R, Strous M, Jetten M, Butler M, Forde R, Fuerst J. 2001. Cell compartmentalisation in planctomycetes: Novel types of structural organisation for the bacterial cell. Arch Microbiol **175**: 413–429.
[7] R. Heald, O. Cohen-Fix, Morphology and function of membrane-bound organelles. *Curr. Opin. Cell Biol*. **26**, 79–86 (2014).
[8] Hyman AA, Weber CA, Jülicher F. Liquid-liquid phase separation in biology. Annu Rev Cell Dev Biol. 2014;30:39-58. doi: 10.1146/annurev-cellbio-100913-013325. PMID: 25288112.
[9] Miller O. L., Hamkalo B. A., Thomas C. A. (1970). Visualization of bacterial genes in action. Science 169, 392–395. 10.1126/science.169.3943.392
[10] Irastortza-Olaziregi M, Amster-Choder O. Coupled Transcription-Translation in Prokaryotes: An Old Couple With New Surprises. Front Microbiol. 2021 Jan 21;11:624830. doi: 10.3389/fmicb.2020.624830. PMID: 33552035; PMCID: PMC7858274.
[11] Papantonis, A. & Cook, P. R. Transcription factories: genome organization and gene regulation. *Chem. Rev.* **113**, 8683–8705 (2013)
[12] Querido, B., Díaz-López, I., & Ramakrishnan, V. (2023). The molecular basis of translation initiation and its regulation in eukaryotes.. *Nature reviews. Molecular cell biology*. https://doi.org/10.1038/s41580-023-00624-9.
[13] Vorländer, M., Pacheco-Fiallos, B., & Plaschka, C. (2022). Structural basis of mRNA maturation: Time to put it together.. *Current opinion in structural biology*, 75, 102431 . https://doi.org/10.1016/j.sbi.2022.102431.
[14] Liu, Y., Bisio, H., Toner, C., Jeudy, S., Philippe, N., Zhou, K., Bowerman, S., White, A., Edwards, G., Abergel, C., & Luger, K. (2021). Virus-encoded histone doublets are essential and form nucleosome-like structures. *Cell*, 184, 4237 - 4250.e19. https://doi.org/10.1016/j.cell.2021.06.032.
[15] Chaikeeratisak, V. et al.. Assembly of a nucleus-like structure during viral replication in bacteria. *Science* **355**, 194–197 (2017).
[16] Rigou S, Schmitt A, Lartigue A, Danner L, Giry C, Trabelsi F, Belmudes L, Olivero-Deibe N, Couté Y, Berois M, Legendre M, Jeudy S, Abergel C, Bisio H. 2024. Nucleocytoviricota viral factories are transient organelles made by phase separation. *bioRxiv*
[17] Modrow S, Falke D, Truyen U, Schätzl H. Viruses: Definition, Structure, Classification. Molecular Virology. 2013 Aug 12:17–30. doi: 10.1007/978-3-642-20718-1_2. PMCID: PMC7123905.
[18] Lwoff A. (1957). The concept of virus. J. Gen. Microbiol. 17, 239–253. 10.1099/00221287-17-2-239
[19] R- Birtles et al., Lancet 349, 925 (1997).
[20] Bernard La Scola *et al.*., A Giant Virus in Amoebae. *Science***299**,20332033(2003).DOI:10.1126/science.1081867
[21] Raoult D, Audic S, Robert C, Abergel C, Renesto P, Ogata H, La Scola B, Suzan M, Claverie JM. The 1.2-megabase genome sequence of Mimivirus. Science. 2004 Nov 19;306(5700):1344-50. doi: 10.1126/science.1101485. Epub 2004 Oct 14. PMID: 15486256.
[22] Rolland C, Andreani J, Louazani AC, Aherfi S, Francis R, Rodrigues R, Silva LS, Sahmi D, Mougari S, Chelkha N, Bekliz M, Silva L, Assis F, Dornas F, Khalil JYB, Pagnier I, Desnues C, Levasseur A, Colson P, Abrahão J, La Scola B. Discovery and Further Studies on Giant Viruses at the IHU Mediterranee Infection That Modified the Perception of the Virosphere. Viruses. 2019 Mar 30;11(4):312. doi: 10.3390/v11040312. PMID: 30935049; PMCID: PMC6520786.
[23] Koonin EV, Dolja VV, Krupovic M, Varsani A, Wolf YI, Yutin N, Zerbini M, Kuhn JH (October 2019). "Create a megataxonomic framework, filling all principal taxonomic ranks, for DNA viruses encoding vertical jelly roll-type major capsid proteins". *ICTV Proposal (Taxoprop)*: 2019.003G. doi:10.13140/RG.2.2.14886.47684.

[24] Aylward, F., Moniruzzaman, M., Ha, A., & Koonin, E. (2021). A phylogenomic framework for charting the diversity and evolution of giant viruses. *PLoS Biology*, 19. https://doi.org/10.1101/2021.05.05.442809.
[25] Schulz, F., Roux, S., Paez-Espino, D. *et al.*. Giant virus diversity and host interactions through global metagenomics. *Nature* **578**, 432–436 (2020). https://doi.org/10.1038/s41586-020-1957-x
[26] Fabre E., Jeudy S., Santini S., Legendre M., Trauchessec M., Couté Y., et al.. (2017). Noumeavirus replication relies on a transient remote control of the host nucleus. *Nat. Commun.* 8:15087. 10.1038/ncomms15087
[27] Ballester M, Galindo-Cardiel I, Gallardo C, Argilaguet JM, Segalés J, Rodriguez JM, and Rodriguez F. 2010. Intranuclear detection of African swine fever virus DNA in several cell types from formalin-fixed and paraffin-embedded tissues using a new in situ hybridization protocol. *J. Virol. Methods* 168:38–43.
[28] Fridmann-Sirkis Y, Milrot E, Mutsafi Y, Ben-Dor S, Levin Y, Savidor A, Kartvelishvily E, Minsky A. Efficiency in Complexity: Composition and Dynamic Nature of Mimivirus Replication Factories. J Virol. 2016 Oct 14;90(21):10039-10047. doi: 10.1128/JVI.01319-16. PMID: 27581975; PMCID: PMC5068508.
[29] Silva LCF, Rodrigues RAL, Oliveira GP, Dornas FP, La Scola B, Kroon EG, Abrahão JS. Microscopic Analysis of the *Tupanvirus* Cycle in *Vermamoeba vermiformis*. Front Microbiol. 2019 Apr 3;10:671. doi: 10.3389/fmicb.2019.00671. PMID: 31001237; PMCID: PMC6456662.
[30] Yoshikawa G, Blanc-Mathieu R, Song C, Kayama Y, Mochizuki T, Murata K, Ogata H, Takemura M. Medusavirus, a Novel Large DNA Virus Discovered from Hot Spring Water. J Virol. 2019 Apr 3;93(8):e02130-18. doi: 10.1128/JVI.02130-18. PMID: 30728258; PMCID: PMC6450098.
[31] Philippe, N. et al.. Pandoraviruses: amoeba viruses with genomes up to 2.5 Mb reaching that of parasitic eukaryotes. *Science* **341**, 281–286 (2013).
[32] C. Abergel, M. Legendre, J.-M. Claverie
The rapidly expanding universe of giant viruses: Mimivirus, Pandoravirus, Pithovirus and Mollivirus
FEMS Microbiol Rev, 39 (2015), pp. 779-796
[33] Zauberman N, Mutsafi Y, Halevy DB, Shimoni E, Klein E, Xiao C, Sun S, Minsky A. Distinct DNA exit and packaging portals in the virus Acanthamoeba polyphaga mimivirus. PLoS Biol. 2008 May 13;6(5):e114. doi: 10.1371/journal.pbio.0060114. PMID: 18479185; PMCID: PMC2430901.
[34] Y. Mutsafi, N. Zauberman, I. Sabanay, & A. Minsky, Vaccinia-like cytoplasmic replication of the giant Mimivirus, Proc. Natl. Acad. Sci. U.S.A. 107 (13) 5978-5982, https://doi.org/10.1073/pnas.0912737107 (2010).
[35] Mutsafi Y, Shimoni E, Shimon A, Minsky A. Membrane assembly during the infection cycle of the giant Mimivirus. PLoS Pathog. 2013;9(5):e1003367. doi: 10.1371/journal.ppat.1003367. Epub 2013 May 30. PMID: 23737745; PMCID: PMC3667779.
[36] *Nucleocytoviricota* viral factories are transient organelles made by liquid-liquid phase separation
Sofia Rigou, Alain Schmitt, Anaísa
B Moreno, Audrey Lartigue, Lucile Danner, Claire Giry, Feres Trabelsi, Lucid Belmudes, Natalia Olivero-Deibe, Hugo
Le Guenno, Yohann Couté, Mabel Berois, Matthieu Legendre, Sandra Jeudy, Chantal Abergel, Hugo Bisio
bioRxiv 2024.09.01.610734; doi: https://doi.org/10.1101/2024.09.01.610734
[37] Rigou S, Schmitt A, Lartigue A, Danner L, Giry C, Trabelsi F, Belmudes L, Olivero-Deibe N, Couté Y, Berois M, Legendre M, Jeudy S, Abergel C, Bisio H. 2024. Nucleocytoviricota viral factories are transient organelles made by phase separation. *bioRxiv*
[38] *Nucleocytoviricota* viral factories are transient organelles made by phase separation
Sofia Rigou, Alain Schmitt, Audrey Lartigue, Lucile Danner, Claire Giry, Feres Trabelsi, Lucid Belmudes, Natalia Olivero-
Deibe, Yohann Couté, Mabel Berois, Matthieu Legendre, Sandra Jeudy, Chantal Abergel, Hugo Bisio
[39] Y. Mutsafi, N. Zauberman, I. Sabanay, & A. Minsky, Vaccinia-like cytoplasmic replication of the giant Mimivirus, Proc. Natl. Acad. Sci. U.S.A. 107 (13) 5978-5982, https://doi.org/10.1073/pnas.0912737107 (2010).
[40] Suzan-Monti, M., Scola, B., Barrassi, L., Espinosa, L., & Raoult, D. (2007). Ultrastructural Characterization of the Giant Volcano-like Virus Factory of Acanthamoeba polyphaga Mimivirus. *PLoS ONE*, 2. https://doi.org/10.1371/journal.pone.0000328.
[41] Mutsafi Y, Shimoni E, Shimon A, Minsky A. Membrane assembly during the infection cycle of the giant Mimivirus. PLoS Pathog. 2013;9(5):e1003367. doi: 10.1371/journal.ppat.1003367. Epub 2013 May 30. PMID: 23737745; PMCID: PMC3667779.

[42] Rigou S, Schmitt A, Lartigue A, Danner L, Giry C, Trabelsi F, Belmudes L, Olivero-Deibe N, Couté Y, Berois M, Legendre M, Jeudy S, Abergel C, Bisio H. 2024. Nucleocytoviricota viral factories are transient organelles made by phase separation. *bioRxiv*

[43] Rippe K. (2022). Liquid-Liquid Phase Separation in Chromatin. *Cold Spring Harbor perspectives in biology*, *14*(2), a040683. https://doi.org/10.1101/cshperspect.a040683

[44] Liu Y, Bisio H, Toner CM, Jeudy S, Philippe N, Zhou K, Bowerman S, White A, Edwards G, Abergel C, Luger K. Virus-encoded histone doublets are essential and form nucleosome-like structures. Cell. 2021 Aug 5;184(16):4237-4250.e19. doi: 10.1016/j.cell.2021.06.032. Epub 2021 Jul 22. PMID: 34297924; PMCID: PMC8357426.)

[45] Liu Y, Bisio H, Toner CM, Jeudy S, Philippe N, Zhou K, Bowerman S, White A, Edwards G, Abergel C, Luger K. Virus-encoded histone doublets are essential and form nucleosome-like structures. Cell. 2021 Aug 5;184(16):4237-4250.e19. doi: 10.1016/j.cell.2021.06.032. Epub 2021 Jul 22. PMID: 34297924; PMCID: PMC8357426.)

[46] Bekliz M, Azza S, Seligmann H, Decloquement P, Raoult D, La Scola B.2018.Experimental Analysis of Mimivirus Translation Initiation Factor 4a Reveals Its Importance in Viral Protein Translation during Infection of Acanthamoeba polyphaga. J Virol92:10.1128/jvi.00337-18.https://doi.org/10.1128/jvi.00337-18

[47] Benarroch, D., Smith, P., & Shuman, S. (2008). Characterization of a trifunctional mimivirus mRNA capping enzyme and crystal structure of the RNA triphosphatase domain. *Structure (London, England : 1993)*, *16*(4), 501–512. https://doi.org/10.1016/j.str.2008.01.009

[48] Boratto, P., Dornas, F., Da Silva, L., Rodrigues, R., Oliveira, G., Cortines, J., Drumond, B., & Abrahão, J. (2017). Analyses of the Kroon Virus Major Capsid Gene and Its Transcript Highlight a Distinct Pattern of Gene Evolution and Splicing among Mimiviruses. *Journal of Virology*, 92. https://doi.org/10.1128/JVI.01782-17.

[49] Hyman AA, Weber CA, Jülicher F. Liquid-liquid phase separation in biology. Annu Rev Cell Dev Biol. 2014;30:39-58. doi: 10.1146/annurev-cellbio-100913-013325. PMID: 25288112.

[50] Gurumurthy A., et al.. Phase separation and transcription regulation: are super-enhancers and Locus control regions primary sites of transcription complex assembly? Bioessays. 2019;41(1) doi: 10.1002/bies.201800164.

[51] Hyman, A.A.; Simons, K. Cell biology. Beyond oil and water--phase transitions in cells. *Science* **2012**, *337*, 1047–1049

[52] Hyman AA, Weber CA, Jülicher F. Liquid-liquid phase separation in biology. Annu Rev Cell Dev Biol. 2014;30:39-58. doi: 10.1146/annurev-cellbio-100913-013325. PMID: 25288112.

[53] Li P., et al.. Phase transitions in the assembly of multivalent signalling proteins. Nature. 2012;483(7389):336–340. doi: 10.1038/nature10879

[54] Xie Q., et al.. Phase separation in cancer at a glance. J. Transl. Med. 2023;21(1):237. doi: 10.1186/s12967-023-04082-x

[55] Patel A., et al.. A liquid-to-solid phase transition of the ALS protein FUS accelerated by disease mutation. Cell. 2015;162(5):1066–1077. doi: 10.1016/j.cell.2015.07.047

[56] Protter DSW, Rao BS, Van Treeck B, Lin Y, Mizoue L, Rosen MK, Parker R. Intrinsically Disordered Regions Can Contribute Promiscuous Interactions to RNP Granule Assembly. Cell Rep. 2018 Feb 6;22(6):1401-1412. doi: 10.1016/j.celrep.2018.01.036. PMID: 29425497; PMCID: PMC5824733.

[57] Borcherds W, Bremer A, Borgia MB, Mittag T. How do intrinsically disordered protein regions encode a driving force for liquid-liquid phase separation? Curr Opin Struct Biol. 2021 Apr;67:41-50. doi: 10.1016/j.sbi.2020.09.004. Epub 2020 Oct 15. PMID: 33069007; PMCID: PMC8044266.

[58] Hughes MP, Sawaya MR, Boyer DR, Goldschmidt L, Rodriguez JA, Cascio D, Chong L,Gonen T, Eisenberg DS: Atomic structures of low-complexity protein segments reveal kinked beta sheets that assemble networks. Science 2018, 359:698–701.

[59] Kato M, Han TNW, Xie SH, Shi K, Du XL, Wu LC, Mirzaei H, Goldsmith EJ, Longgood J, Pei JM, et al.. : Cell-free Formation of RNA Granules: Low Complexity Sequence Domains Form Dynamic Fibers within Hydrogels. Cell 2012, 149:753–767.

[60] Yoshizawa T, Nozawa RS, Jia TZ, Saio T, Mori E. Biological phase separation: cell biology meets biophysics. Biophys Rev. 2020 Apr;12(2):519-539. doi: 10.1007/s12551-020-00680-x. Epub 2020 Mar 18. PMID: 32189162; PMCID: PMC7242575.

[61] Tsang B, Arsenault J, Vernon RM, Lin H, Sonenberg N, Wang LY, Bah A, Forman-Kay JD: Phosphoregulated FMRP phase separation models activity-dependent translation through bidirectional control of mRNA granule formation. Proc Natl Acad Sci U S A 2019, 116:4218–4227.

[62] Nott TJ, Petsalaki E, Farber P, Jervis D, Fussner E, Plochowietz A, Craggs TD, Bazett-Jones DP, Pawson T, Forman-Kay JD, et al.. : Phase transition of a disordered nuage protein generates environmentally responsive membraneless organelles. Mol Cell 2015, 57:936–947.
[63] Dunker AK, Cortese MS, Romero P, Iakoucheva LM, Uversky VN: Flexible nets. The roles of intrinsic disorder in protein interaction networks. FEBS J 2005, 272:5129–5148
[64] Xu B, He G, Weiner BG, Ronceray P, Meir Y, Jonikas MC, Wingreen NS: Rigidity enhances a magic-number effect in polymer phase separation. Nature Communications 2020, 11:1561
[65] Jackson, D. A., Hassan, A. B., Errington, R. J. & Cook, P. R. Visualization of focal sites of transcription within human nuclei. *EMBO J.* **12**, 1059–1065 (1993).
[66] Papantonis, A. & Cook, P. R. Transcription factories: genome organization and gene regulation. *Chem. Rev.* **113**, 8683–8705 (2013)
[67] Iborra FJ, Pombo A, Jackson DA, et al.. Active RNA polymerases are localized within discrete transcription "factories' in human nuclei. J Cell Sci. 1996;109(6):1427–1436
[68] Banani, S. F., Lee, H. O., Hyman, A. A. & Rosen, M. K. Biomolecular condensates: organizers of cellular biochemistry. *Nat. Rev. Mol. Cell Biol.* **18**, 285–298 (2017)
[69] Boija, A. et al.. Transcription factors activate genes through the phase-separation capacity of their activation domains. *Cell* **175**, 1842–1855.e16 (2018).
[70] A. Ladouceur, B.S. Parmar, S. Biedzinski, J. Wall, S.G. Tope, D. Cohn, A. Kim, N. Soubry, R. Reyes-Lamothe, & S.C. Weber, Clusters of bacterial RNA polymerase are biomolecular condensates that assemble through liquid–liquid phase separation, Proc. Natl. Acad. Sci. U.S.A. 117 (31) 18540-18549, https://doi.org/10.1073/pnas.2005019117 (2020).
[71] Rada-Iglesias A., Grosveld F.G., Papantonis A. Forces driving the three-dimensional folding of eukaryotic genomes. Mol. Syst. Biol. 2018;14:e8214. doi: 10.15252/msb.20188214.
[72] Li, X., An, Z., Zhang, W., & Li, F. (2023). Phase Separation: Direct and Indirect Driving Force for High-Order Chromatin Organization. *Genes*, *14*(2), 499. https://doi.org/10.3390/genes14020499
[73] Alenquer, M.; Vale-Costa, S.; Etibor, T.A.; Ferreira, F.; Sousa, A.L.; Amorim, M.J. Influenza A virus ribonucleoproteins form liquid organelles at endoplasmic reticulum exit sites. *Nat. Commun.* **2019**, *10*, 1629
[74] Chen, H.; Cui, Y.; Han, X.; Hu, W.; Sun, M.; Zhang, Y.; Wang, P.H.; Song, G.; Chen, W.; Lou, J. Liquid-liquid phase separation by SARS-CoV-2 nucleocapsid protein and RNA. *Cell Res.* **2020**, *30*, 1143–1145
[75] Zhou, Y.; Su, J.M.; Samuel, C.E.; Ma, D. Measles Virus Forms Inclusion Bodies with Properties of Liquid Organelles. *J. Virol.* **2019**, *93*, 10
[76] Rigou S, Schmitt A, Lartigue A, Danner L, Giry C, Trabelsi F, Belmudes L, Olivero-Deibe N, Couté Y, Berois M, Legendre M, Jeudy S, Abergel C, Bisio H. 2024. Nucleocytoviricota viral factories are transient organelles made by phase separation. *bioRxiv*
[77] Rigou S, Schmitt A, Lartigue A, Danner L, Giry C, Trabelsi F, Belmudes L, Olivero-Deibe N, Couté Y, Berois M, Legendre M, Jeudy S, Abergel C, Bisio H. 2024. Nucleocytoviricota viral factories are transient organelles made by phase separation. *bioRxiv*
[78] Rigou S, Schmitt A, Lartigue A, Danner L, Giry C, Trabelsi F, Belmudes L, Olivero-Deibe N, Couté Y, Berois M, Legendre M, Jeudy S, Abergel C, Bisio H. 2024. Nucleocytoviricota viral factories are transient organelles made by phase separation. *bioRxiv*
[79] Mutsafi Y, Zauberman N, Sabanay I, Minsky A. 2010. Vaccinia-like cytoplasmic replication of the giant Mimivirus. *Proc Natl Acad Sci USA* 107:5978–5982.
[80] Mutsafi Y, Zauberman N, Sabanay I, Minsky A. 2010. Vaccinia-like cytoplasmic replication of the giant Mimivirus. *Proc Natl Acad Sci USA* 107:5978–5982.
[81] Mutsafi Y, Zauberman N, Sabanay I, Minsky A. 2010. Vaccinia-like cytoplasmic replication of the giant Mimivirus. *Proc Natl Acad Sci USA* 107:5978–5982.
[82] Legendre M, Audic S, Poirot O, Hingamp P, Seltzer V, Byrne D, Lartigue A, Lescot M, Bernadac A, Poulain J, Abergel C, Claverie J-M. 2010. mRNA deep sequencing reveals 75 new genes and a complex transcriptional landscape in Mimivirus. *Genome Res* 20:664–674.
[83] Mayer L, Nikolov G, Kunert M, Horn M, Willemsen A. 2025. Mimivirus transcription and translation occur at well-defined locations within amoeba host cells. J Virol 99:e00554-25. https://doi.org/10.1128/jvi.00554-25
[84] Dieterich DC, Link AJ, Graumann J, Tirrell DA, Schuman EM. 2006. Selective identification of newly synthesized proteins in mammalian cells using bioorthogonal noncanonical amino acid tagging (BONCAT). *Proc Natl Acad Sci USA* 103:9482–9487.
[85] Hatzenpichler R, Orphan VJ. 2016. Detection of protein-synthesizing microorganisms in the environment via Bioorthogonal Noncanonical Amino Acid Tagging (BONCAT), p 145–157. In McGenity TJ, Timmis KN,

Nogales B (ed), *Hydrocarbon and lipid microbiology protocols: single-cell and single-molecule methods*. Springer, Berlin, Heidelberg.
[86] Pasulka AL, Thamatrakoln K, Kopf SH, Guan Y, Poulos B, Moradian A, Sweredoski MJ, Hess S, Sullivan MB, Bidle KD, Orphan VJ. 2018. Interrogating marine virus-host interactions and elemental transfer with BONCAT and nanoSIMS-based methods. *Environ Microbiol* 20:671–692.
[87] Dieterich DC, Hodas JJL, Gouzer G, Shadrin IY, Ngo JT, Triller A, Tirrell DA, Schuman EM. 2010. In situ visualization and dynamics of newly synthesized proteins in rat hippocampal neurons. *Nat Neurosci* 13:897–905.
[88] Iwasaki S, Ingolia NT. 2017. The growing toolbox for protein synthesis studies. *Trends Biochem Sci* 42:612–624.
[89] Mayer L, Nikolov G, Kunert M, Horn M, Willemsen A. 2025. Mimivirus transcription and translation occur at well-defined locations within amoeba host cells. J Virol 99:e00554-25. https://doi.org/10.1128/jvi.00554-25
[90] Willemsen A, Manzano-Marín A, Horn M. 2025. Novel high-quality amoeba genomes reveal widespread codon usage mismatch between giant viruses and their hosts. *Genome Biol Evol* 17:evae271.
[91] Bae, H. & Coller, J. Codon optimality-mediated mRNA degradation: Linking translational elongation to mRNA stability. Molecular Cell **82**, 1467–1476 (2022).
[92] Zhang R, Mayer L, Hikida H, Shichino Y, Mito M, Willemsen A, Iwasaki S, Ogata H. 2024. Giant virus creates subcellular environment to overcome codon– tRNA mismatch. *bioRxiv*.
[93] Zhang R, Mayer L, Hikida H, Shichino Y, Mito M, Willemsen A, Iwasaki S, Ogata H. 2024. Giant virus creates subcellular environment to overcome codon– tRNA mismatch. *bioRxiv*.
[94] Mutsafi Y, Shimoni E, Shimon A, Minsky A. 2013. Membrane assembly during the infection cycle of the giant Mimivirus. *PLoS Pathog* 9:e1003367.
[95] *Nucleocytoviricota* viral factories are transient organelles made by phase separation
Sofia Rigou, Alain Schmitt, Audrey Lartigue, Lucile Danner, Claire Giry, Feres Trabelsi, Lucid Belmudes, Na talia Olivero-
Deibe, Yohann Couté, Mabel Berois, Matthieu Legendre, Sandra Jeudy, Chantal Abergel, Hugo Bisio
[96] Rigou S, Schmitt A, Lartigue A, Danner L, Giry C, Trabelsi F, Belmudes L, Olivero-Deibe N, Couté Y, Berois M, Legendre M, Jeudy S, Abergel C, Bisio H. 2024. Nucleocytoviricota viral factories are transient organelles made by phase separation. *bioRxiv*
[97] Rigou S, Schmitt A, Lartigue A, Danner L, Giry C, Trabelsi F, Belmudes L, Olivero-Deibe N, Couté Y, Berois M, Legendre M, Jeudy S, Abergel C, Bisio H. 2024. Nucleocytoviricota viral factories are transient organelles made by phase separation. *bioRxiv*
[98] Rigou S, Schmitt A, Lartigue A, Danner L, Giry C, Trabelsi F, Belmudes L, Olivero-Deibe N, Couté Y, Berois M, Legendre M, Jeudy S, Abergel C, Bisio H. 2024. Nucleocytoviricota viral factories are transient organelles made by phase separation. *bioRxiv*
[99] Y. Mutsafi, N. Zauberman, I. Sabanay, & A. Minsky, Vaccinia-like cytoplasmic replication of the giant Mimivirus, Proc. Natl. Acad. Sci. U.S.A. 107 (13) 5978-5982, https://doi.org/10.1073/pnas.0912737107 (2010).
[100] Mutsafi Y, Zauberman N, Sabanay I, Minsky A. 2010. Vaccinia-like cytoplasmic replication of the giant Mimivirus. *Proc Natl Acad Sci USA* 107:5978–5982.
[101] Mayer L, Nikolov G, Kunert M, Horn M, Willemsen A. 2025. Mimivirus transcription and translation occur at well-defined locations within amoeba host cells. J Virol 99:e00554-25. https://doi.org/10.1128/jvi.00554-25
[102] Vincent F, Sheyn U, Porat Z, Schatz D, Vardi A. 2021. Visualizing active viral infection reveals diverse cell fates in synchronized algal bloom demise. *Proc Natl Acad Sci USA* 118:e2021586118.
[103] Altschul SF, Gish W, Miller W, Myers EW, Lipman DJ. 1990. Basic local alignment search tool. *J Mol Biol* 215:403–410.